iScience

CellPress
OPEN ACCESS

Article

Restored autophagy is protective against PAK3-induced cardiac dysfunction

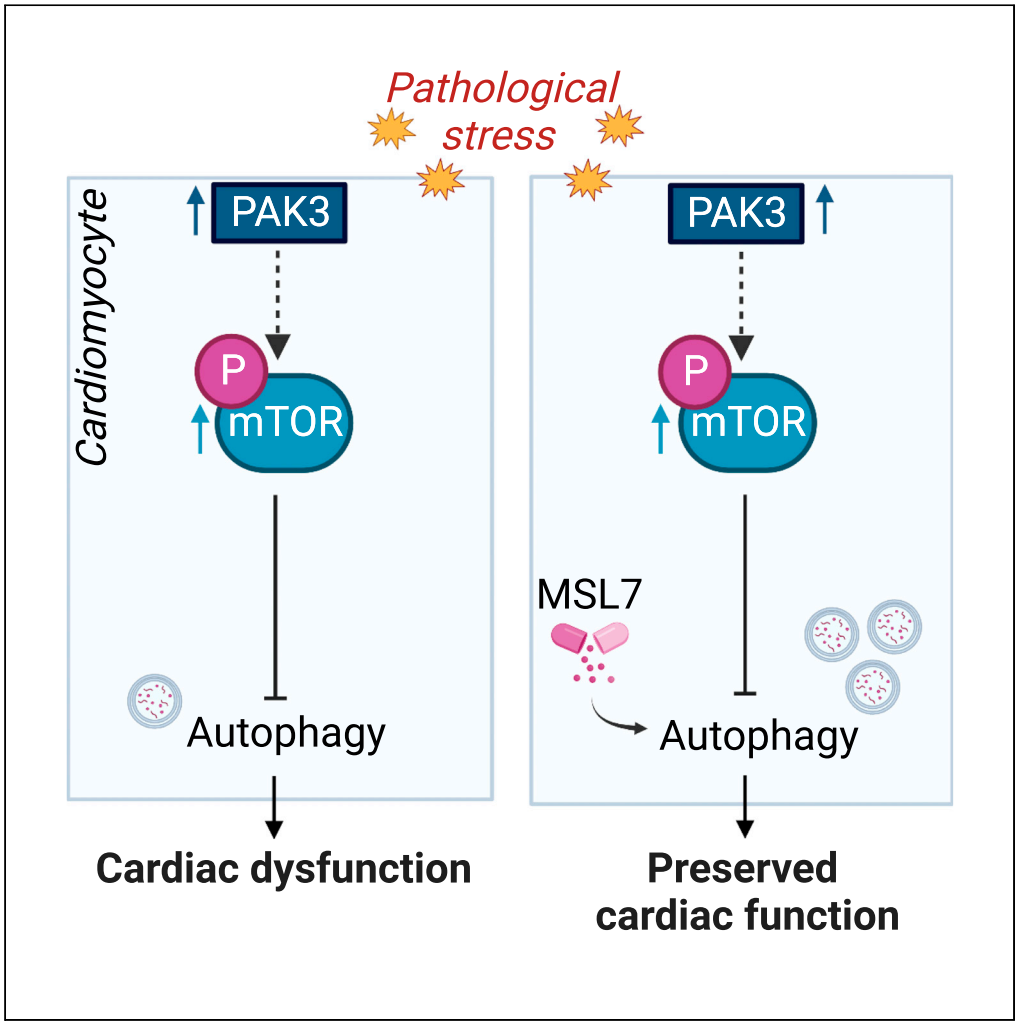

Andrea Ruiz-Velasco, Rida Raja, Xinyi Chen, ..., Oliver J. Müller, Elizabeth J. Cartwright, Wei Liu

wei.liu@manchester.ac.uk

Highlights

PAK3 expression and phosphorylation is increased in failing hearts

Cardiac PAK3 overexpression impairs heart function with isoprenaline stress

PAK3 downregulates cardiac autophagy by interacting with mTORC1 pathway

MSL-7 maintains heart function by preserving autophagy

Ruiz-Velasco et al., iScience *26*, 106970
June 16, 2023 © 2023
https://doi.org/10.1016/j.isci.2023.106970

iScience

CellPress
OPEN ACCESS

Article

Restored autophagy is protective against PAK3-induced cardiac dysfunction

Andrea Ruiz-Velasco,[1] Rida Raja,[1] Xinyi Chen,[1] Haresh Ganenthiran,[1] Namrita Kaur,[1] Nasser hawimel o Alatawi,[1] Jessica M. Miller,[2] Riham R.E. Abouleisa,[2] Qinghui Ou,[2] Xiangjun Zhao,[1] Oveena Fonseka,[1] Xin Wang,[1] Susanne S. Hille,[3,4] Norbert Frey,[3,4] Tao Wang,[1] Tamer M.A. Mohamed,[2] Oliver J. Müller,[3,4] Elizabeth J. Cartwright,[1] and Wei Liu[1,5,*]

SUMMARY

Despite the development of clinical treatments, heart failure remains the leading cause of mortality. We observed that p21-activated kinase 3 (PAK3) was augmented in failing human and mouse hearts. Furthermore, mice with cardiac-specific PAK3 overexpression exhibited exacerbated pathological remodeling and deteriorated cardiac function. Myocardium with PAK3 overexpression displayed hypertrophic growth, excessive fibrosis, and aggravated apoptosis following isoprenaline stimulation as early as two days. Mechanistically, using cultured cardiomyocytes and human-relevant samples under distinct stimulations, we, for the first time, demonstrated that PAK3 acts as a suppressor of autophagy through hyper-activation of the mechanistic target of rapamycin complex 1 (mTORC1). Defective autophagy in the myocardium contributes to the progression of heart failure. More importantly, PAK3-provoked cardiac dysfunction was mitigated by administering an autophagic inducer. Our study illustrates a unique role of PAK3 in autophagy regulation and the therapeutic potential of targeting this axis for heart failure.

INTRODUCTION

Heart failure remains the leading cause of mortality, despite robust successes in its treatment. Constant cardiac hypertrophic growth contributes to the transition to heart failure. Unbalanced protein synthesis and degradation lead to progressive hypertrophy of the myocardium[1]; however, the underlying molecular basis and the relevant treatment feasibility to prevent heart failure are largely unknown. Therefore, further identification of the mechanisms whereby protein homeostasis is regulated in cardiomyocytes under stress is necessitated to exploit novel drug targets.

Autophagy is a dynamic intracellular process that mediates protein degradation, organelle turnover, and cytoplasmic component recycling during nutrient starvation and pathological stress.[2–4] It is acknowledged that autophagy exhibits a dual role in the heart: adaptive autophagy is initiated in the myocardium to tackle protein aggregates, energetic deprivation, oxidative stress, cell death, and mitochondrial dysfunction in response to short-term pathological stress,[5–9] whereas prolonged stimulation eventually induces maladaptive autophagic activity, resulting in the onset and development of heart failure.[10–12] Therefore, the study of cardiac autophagy sheds light on its implications and opportunities for treating heart failure.

The mechanistic target of rapamycin complex 1 (mTORC1) is a key regulator of autophagy in cardiomyocytes.[13,14] In the heart, mTORC1 is required for cell growth and is also known as a major regulator of autophagy.[15,16] Unc-51 like autophagy activating kinase 1 (ULK1), the mammalian ortholog of autophagy-related protein 1), is critical for autophagy initiation by recruiting autophagy-related proteins to the autophagosome.[17] The autophagosome formation process comprises nucleation, elongation, and completion steps driven by complex and coordinated molecular signaling engulfing cargos for degradation.[18] Following fusion with the lysosome, the cargo is degraded by the autolysosome.[18] mTORC1 directly inhibits autophagosome formation, for instance, blocking autophagic initiation by phosphorylating ULK1 at the Serine 757,[19] and elongation and completion by influencing autophagy-related proteins as well.[20] In addition, activated mTORC1 hinders the fusion of the autophagosome with the lysosome, subsequently impairing the

[1]Faculty of Biology, Medicine, and Health, University of Manchester, Oxford Road, Manchester M13 9PT, UK

[2]Institute of Molecular Cardiology, University of Louisville, 580 S Preston St, Louisville, KY 40202, USA

[3]Department of Internal Medicine III, University of Kiel, Kiel, Germany

[4]DZHK, German Centre for Cardiovascular Research, Partner Site Hamburg/Kiel/Lübeck, Kiel, Germany

[5]Lead contact

*Correspondence: wei.liu@manchester.ac.uk

https://doi.org/10.1016/j.isci.2023.106970

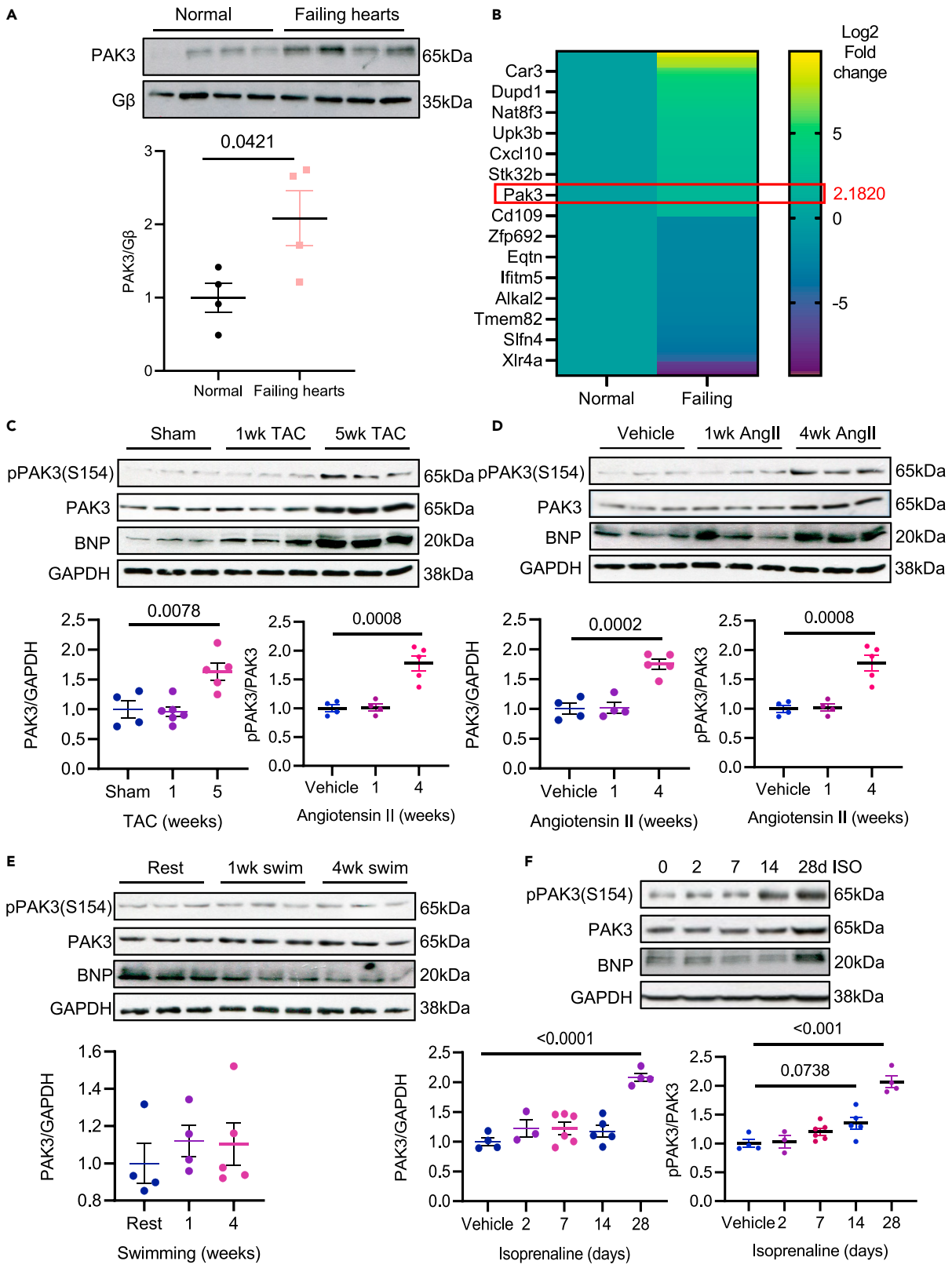
A
Normal
Failing hearts
PAK3
65kDa
Gβ
35kDa
0.0421
PAK3/Gβ
Normal
Failing hearts
B
Log2
Fold
change
Car3
Dupd1
Nat8f3
Upk3b
Cxcl10
Stk32b
Pak3
Cd109
Zfp692
Eqtn
Ifitm5
Alkal2
Tmem82
Slfn4
Xlr4a
2.1820
Normal
Failing
C
Sham
1wk TAC
5wk TAC
pPAK3(S154)
PAK3
BNP
GAPDH
65kDa
20kDa
38kDa
0.0078
PAK3/GAPDH
TAC (weeks)
0.0008
pPAK3/PAK3
Angiotensin II (weeks)
D
Vehicle
1wk AngII
4wk AngII
0.0002
0.0008
E
Rest
1wk swim
4wk swim
Swimming (weeks)
F
0
2
7
14
28d ISO
<0.0001
<0.001
0.0738
Isoprenaline (days)

Figure 1. PAK3 is increased in failing hearts

(A) Immunoblotting analyses of total and phosphorylated PAK3 in human failing hearts. N = 4.

(B) RNA-Seq heatmap showing differentially expressed (DE) genes in the failing hearts. The filtered reads were mapped to the mouse reference sequence set (mm10/Dec. 2011/GRCm38) from the UCSC browser. Gene expression profiling in normal hearts was normalized to light green, which is defined as unchanged. Among ~53,000 genes, 314 DE genes in the failing hearts with $p < 0.05$ and an absolute value of a $\log_2$ fold change of more than 2 were selected.

(C–F) PAK3 phosphorylation, expression, and BNP level in the failing hearts from C57BL/6 mice after long-term TAC stimulation (C), constant Angiotensin II (AngII, 1 mg/kg/day) infusion (D), and ISO-induced (8 mg/kg/day) (F). Representative western blot and quantification for expression and phosphorylation of PAK3, and BNP expression in the hearts from C57BL/6 mice after swimming exercise (E). N = 6–9.

Data presented as mean ± SEM. p values vs. control determined by (A) two-tailed Student's *t* test and by (C-F) One-way ANOVA with Dunnett's post hoc test.

autophagic flux.[20] More importantly, interfering with mTOR activity appears beneficial, maintaining optimal autophagy events and improving cardiac function under pathological stresses.[21–27] As such, it is important to decipher the molecular mechanisms governing mTOR regulation of the autophagic process in the heart to divulge the potential targets for preventing heart failure.

P21-activated kinases (PAKs) are a family of non-receptor serine/threonine kinases, the downstream effectors of the Rho family of GTPases. PAKs are involved in cell survival, proliferation, and cytoskeleton remodeling.[28,29] The mammalian PAKs are classified into two groups based on their sequence, structural homology, and activation regulation: group I (PAK1–3) and group II (PAK4–6).[28,29] Our previous studies revealed the cardioprotective functions of PAK1 and PAK2 in the myocardium. PAK1 protects the heart against pressure overload-induced pathological hypertrophy by preventing nuclear factor of activated T-cells (NFAT)-mediated pro-hypertrophic gene expression and reinforcing Fbxo32-mediated protein degradation.[30–32] Moreover, we demonstrated that PAK2 in cardiomyocytes protects the hearts from pressure overload-induced heart failure by enhancing adaptive endoplasmic reticulum stress response.[33] PAK3 is the least studied group I members. It shares 83% homology of structure with PAK1 and PAK2.[34] Noticeably, its function in cardiomyocytes in response to pathological stress is unexplored.

This study shows that cardiac PAK3 was upregulated in failing human and mouse hearts. In addition, we demonstrate that overexpressed cardiac PAK3 contributes to pathological remodeling and heart failure. Mechanistically, upregulated PAK3 constrained cardiac autophagy likely through the activation of mTOR in both *in vivo* and *in vitro* models under various pathological stresses. On the contrary, the knockdown of PAK3 preserved autophagy, maintaining protein homeostasis and tackling the stress. PAK3 repression of stress-induced autophagy was particularly confirmed in cultured human heart slices and human induced pluripotent stem cell-derived cardiomyocytes (iPSC-CMs) upon stimulation with isoprenaline (ISO) and starvation. In addition, an autophagy inducer, MSL-7, preserved cardiac function in spite of PAK3 overexpression in the heart. In summary, we have unraveled the role of PAK3 in cardiac autophagy, suggesting it contributes to the transition to heart failure because of pathological stresses. We have also provided proof-of-concept evidence of the therapeutic potential of targeting cardiac autophagy.

RESULTS

PAK3 is upregulated in pathological stress-induced failing hearts

To investigate the physio-pathological role of PAK3 in the myocardium, first, we assessed its expression in failing human hearts and detected a higher level of protein (Figure 1A). In addition, RNA-Seq on the failing mouse hearts detected an increase of *Pak3* in pathological stress-induced failing hearts (Figure 1B). Among ~53,000 genes, 314 differentially expressed (DE) genes in the failing hearts with an absolute value of a $\log_2$ fold change of more than two were selected. Pak3 was increased with a $\log_2$ fold change of 2.2. The increased Pak3 indicates that it is likely involved in the pathogenesis of heart failure. Furthermore, we found that PAK3 expression and its phosphorylation levels were increased in the failing hearts from C57BL/6 mice (Figures 1C, 1D, S1A, and S1B), induced by pressure overload stimulation for 5 weeks or constant angiotensin infusion for 4 weeks, although its activation and expression were unchanged under acute stimulation. However, PAK3 phosphorylation and expression remained unchanged regardless of 1 week or 4 weeks of swimming exercise (Figures 1E and S1C), indicating that augmented PAK3 is associated with pathological stresses. Finally, we also evaluated the involvement of PAK3 during the progression of pathological stress-induced heart failure. PAK3 phosphorylation was greater and maintained after 2 weeks of isoprenaline (ISO), and its expression was increased after 4 weeks (Figures 1F and S1D). All the above data suggest that increased PAK3 is likely a maladaptive response to pathological stresses.

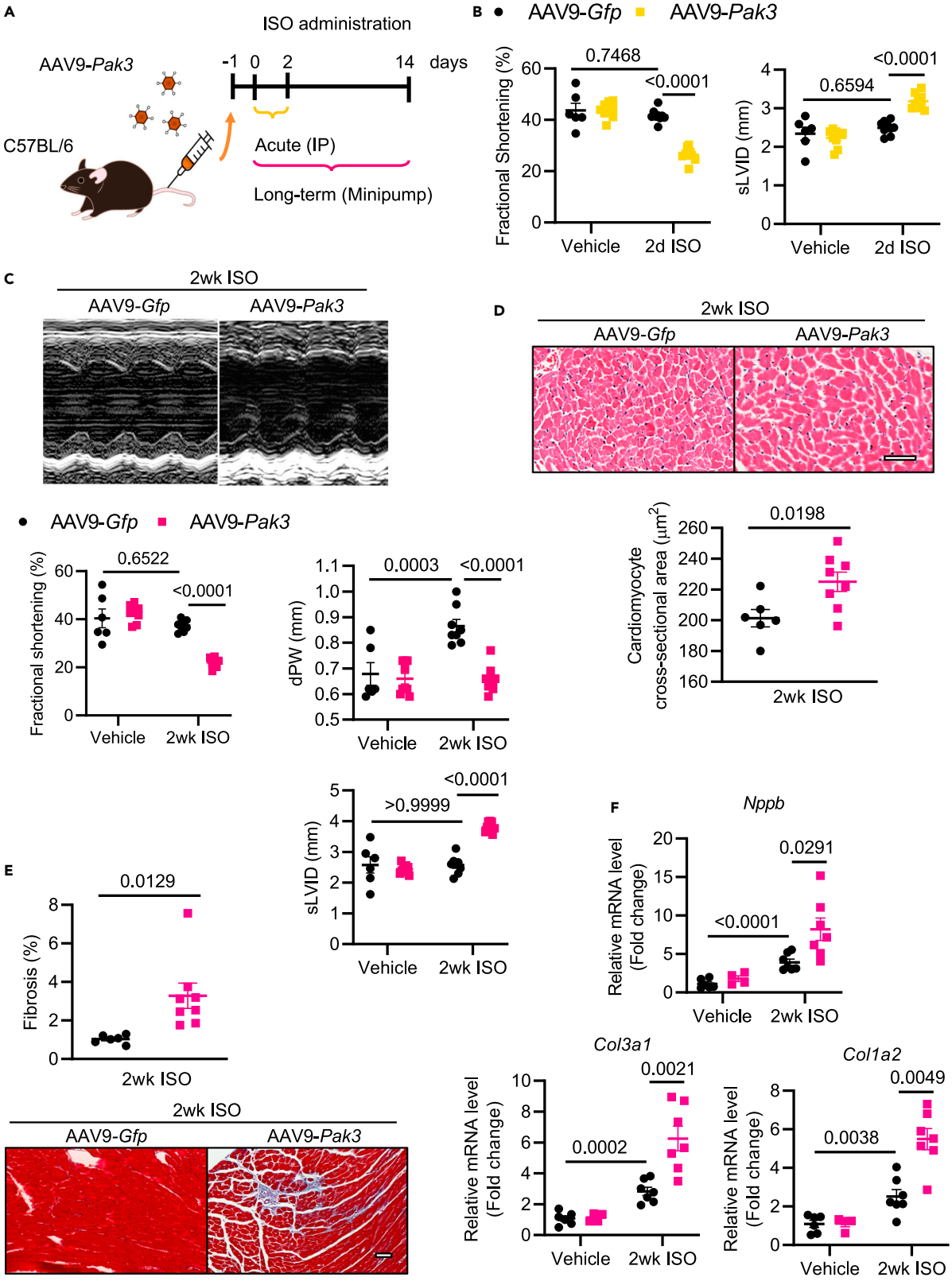
A
ISO administration
AAV9-Pak3
-1 0 2 14 days
C57BL/6
Acute (IP)
Long-term (Minipump)
B
AAV9-Gfp
AAV9-Pak3
Fractional Shortening (%)
0.7468
<0.0001
Vehicle
2d ISO
sLVID (mm)
0.6594
<0.0001
Vehicle
2d ISO
C
2wk ISO
AAV9-Gfp
AAV9-Pak3
D
2wk ISO
AAV9-Gfp
AAV9-Pak3
AAV9-Gfp
AAV9-Pak3
Fractional shortening (%)
0.6522
<0.0001
Vehicle
2wk ISO
dPW (mm)
0.0003
<0.0001
Vehicle
2wk ISO
Cardiomyocyte cross-sectional area (μm²)
0.0198
2wk ISO
sLVID (mm)
<0.0001
>0.9999
Vehicle
2wk ISO
E
Fibrosis (%)
0.0129
2wk ISO
2wk ISO
AAV9-Gfp
AAV9-Pak3
F
Nppb
Relative mRNA level (Fold change)
0.0291
<0.0001
Vehicle
2wk ISO
Col3a1
Relative mRNA level (Fold change)
0.0021
0.0002
Vehicle
2wk ISO
Col1a2
Relative mRNA level (Fold change)
0.0049
0.0038
Vehicle
2wk ISO

Figure 2. PAK3 overexpression induces pathological remodeling and cardiac dysfunction in response to isoprenaline (ISO) stress

(A) Experimental overview of ISO stimulation (8 mg/kg/day) on AAV9-*Pak3* injected 8-week-old male C57BL/6 mice.

(B and C) (B) Fractional shortening (%) and end-systolic left ventricular internal diameter (sLVID) of mice subject to ISO for 2 days (C) Representative left ventricular M-mode echocardiographic images, fractional shortening (%), end-diastolic left ventricular posterior wall thickness (dPW), and sLVID after 2-week ISO stress. N = 6–9.

(D and E) H&E staining for cross-sectional area (D), and Masson's Trichrome images for detecting fibrosis (E) in the heart 2 weeks post-ISO. Scale bar: 50 μm. N = 6–8.

(F) Relative mRNA expression of *Nppb*, *Col3a1*, and *Col1a2*. N = 4–7.

Data presented as mean ± SEM. p values vs. control were determined by (D, E) two-tailed Student's *t-test*, and (B, C, F) multiple comparison p values were calculated by two-way ANOVA with Tukey's correction.

PAK3 induces pathological hypertrophy and heart failure

The upregulation of PAK3 in the failing heart prompted the consideration that PAK3 is possibly a causative factor of cardiac dysfunction. Thus, to test for the plausible link between PAK3 upregulation and the progression of heart failure, we induced cardiomyocyte-specific PAK3 overexpression (Figure S2) by injection of AAV9 delivery of troponin T (TnT) promoter-driven human *Pak3* (AAV9-TnT-*Pak3*, $1x10^{11}$ viral particles) in 8-week-old male C57BL/6 mice. Following constant ISO stimulation (8 mg/kg/day) for 2 days and 2 weeks (Figure 2A), cardiac function and morphologic assessments were performed. First, echocardiography determined that AAV9-TnT-*Pak3* injected mice had systolic cardiac dysfunction compared to control mice (mice with AAV9-TnT-*Gfp* injection) subject to ISO treatment for 2 days, exemplified by a declining fractional shortening (FS%) and distended left ventricular chamber (Figure 2B; Table S1). On this acute pathological stress, PAK3 overexpression did not affect heart weight, lung weight, or hypertrophic growth but increased fibrosis in the myocardium (Figures S3A–S3D).

Meanwhile, during long-term ISO stress (2 weeks), the mice with cardiac PAK3 overexpression displayed reduced FS% and enlarged left ventricular systolic chamber size (Figure 2C). Diastolic and systolic posterior wall thickness were thinner in the PAK3-overexpressed heart, indicating cardiac dilation and heart failure (Figure 2C; Table S2). Concerning pathological hypertrophic remodeling, an enlarged cardiomyocyte cross-sectional area and more interstitial fibrosis were detected in the PAK3-overexpressed myocardium compared to the AAV9-TnT-*Gfp* group following ISO stress (Figures 2D and 2E). The transcripts of the hypertrophic gene markers, brain natriuretic peptide (*Nppb*), and markers of fibrosis, collagen type 3 alpha 1 chain (*Col3a1*) and collagen type 1 alpha 2 chain (*Col1a2*), were also significantly upregulated after 2 weeks ISO stress and PAK3 overexpression (Figure 2F). The above data imply that increased PAK3, at least in part, contributes to pathological stress-induced hypertrophy remodeling and cardiac dysfunction, suggesting a causal link between the upregulation of PAK3 and the onset or progression of heart failure.

PAK3 overexpression promotes cell death by hampering myocardial autophagy

We observed that protein aggregation was evident in PAK3-overexpressed myocardium following 2 weeks ISO, indicated by Crystallin Alpha B (CryAB) staining (Figure 3A). Because CryAB binds misfolded proteins, PAK3 is likely to regulate protein homeostasis. Autophagy is one of the mechanisms activated on pathological stress to prevent aberrant protein aggregation. A delicate regulation of the autophagic process is vital for preserving cardiac function.[35] Therefore, we assessed critical autophagic markers to evaluate whether cardiac PAK3 regulates autophagy in the myocardium. Cytosolic microtubule-associated protein 1A/1B-light chain 3 (LC3) is conjugated to phosphatidylethanolamine to form LC3II, which is incorporated into the membrane of autophagosomes.[36] After two days of ISO stress, an increase of LC3II/LC3I (LC3II/I ratio is a marker of functional autophagy) was observed in control hearts, whereas LC3II/LC3I was not heightened in PAK3-overexpressed myocardium (Figure 3B). Similarly, autophagy-related gene 5 (ATG5) and ATG12 are markers for autophagosome elongation, which was also blunted by PAK3 overexpression (Figure 3B). Moreover, phosphorylation of ULK1 at Serine 555 was reduced, although its total expression was unaltered because of PAK3 overexpression, suggesting PAK3 is a negative regulator of autophagy signaling pathways (Figure 3B). Finally, a corresponding accumulation of sequestosome-1 (SQSTM1, also known as the ubiquitin-binding protein p62, a marker of autophagic degradation) on acute ISO stress was observed in PAK3-overexpressed heart, indicating PAK3-blocked degradation phase of autophagosomes (Figure 3B). This attenuation of autophagy was associated with exaggerated cardiomyocyte apoptosis (Figure 3C).

The inhibitory effect of PAK3 on cardiac autophagy was sustained through long-term ISO stimulation. For instance, a higher level of p62 and lower ATG5-12 were detected in PAK3-overexpressed myocardium

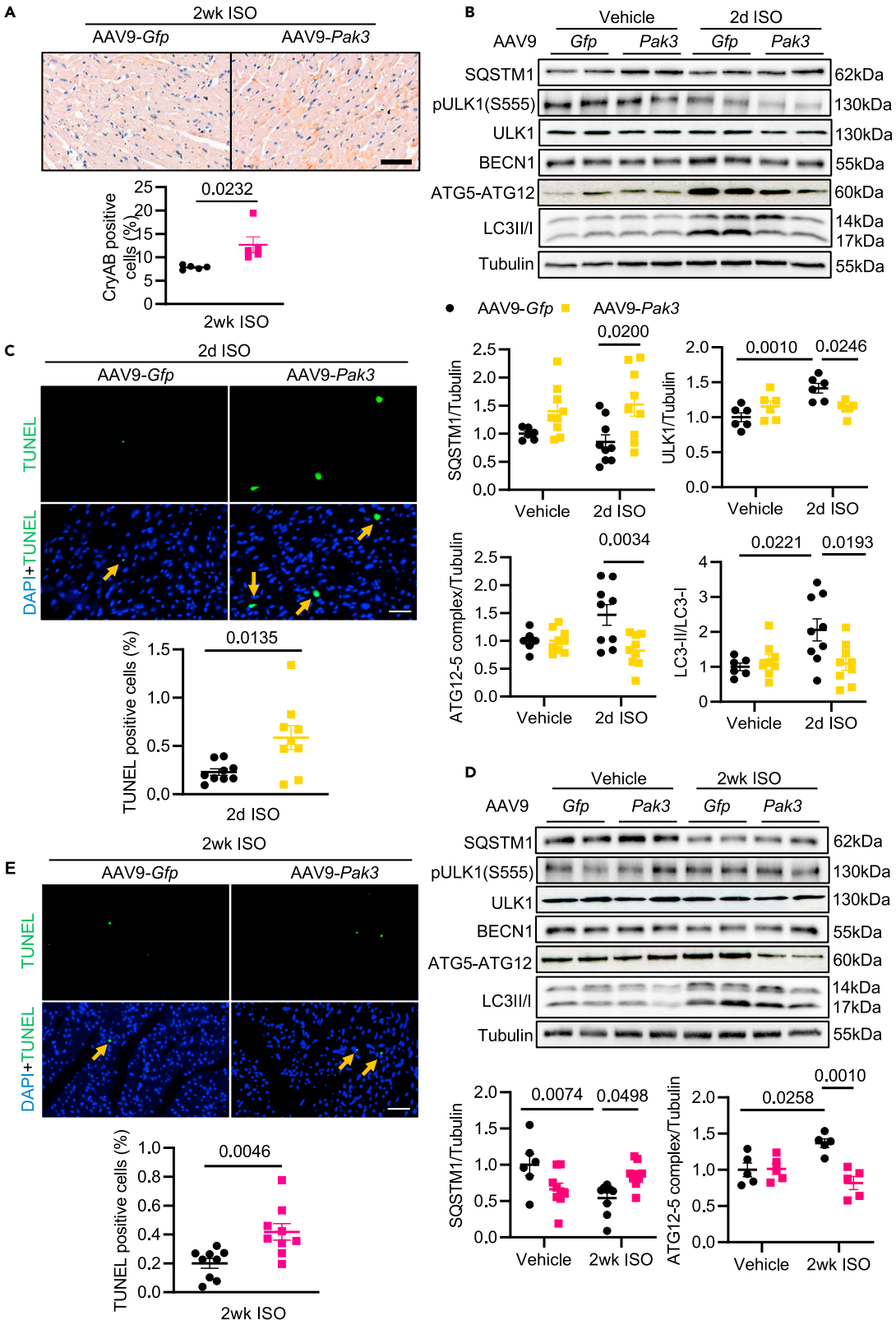
A
2wk ISO
AAV9-Gfp
AAV9-Pak3
CryAB positive cells (%)
0.0232
2wk ISO
B
Vehicle
2d ISO
AAV9
Gfp
Pak3
SQSTM1
pULK1(S555)
ULK1
BECN1
ATG5-ATG12
LC3II/I
Tubulin
62kDa
130kDa
130kDa
55kDa
60kDa
14kDa
17kDa
55kDa
C
2d ISO
TUNEL
DAPI+TUNEL
TUNEL positive cells (%)
0.0135
2d ISO
SQSTM1/Tubulin
0.0200
ULK1/Tubulin
0.0010
0.0246
ATG12-5 complex/Tubulin
0.0034
LC3-II/LC3-I
0.0221
0.0193
Vehicle
2d ISO
D
2wk ISO
E
2wk ISO
TUNEL positive cells (%)
0.0046
2wk ISO
0.0074
0.0498
0.0258
0.0010

Figure 3. Cardiac PAK3 blocks autophagy and promotes cell death

(A) Immunohistochemical staining of CryAB showing protein aggregation in PAK3-overexpressed myocardium after 2 weeks ISO. Scale bar: 50 μm. N = 5.
(B and C) (B) Immunoblots and quantification of autophagic markers in the myocardium, and (C) TUNEL staining indicating apoptosis in cardiomyocytes from mice after 2 days ISO. Scale bar: 50 μm. N = 6–9.
(D and E) (D) Immunoblots and quantification of autophagic markers in the myocardium, and (E) TUNEL staining of the heart subject to 2 weeks ISO stress. Scale bar: 50 μm. N = 6–9.
Data presented as mean ± SEM. p values vs. control were determined by (A, C, E) two-tailed Student's *t-test*, and (B, D) multiple comparison p values were calculated by two-way ANOVA with Tukey's correction.

(Figure 3D). This was accompanied by the induction of cell death in AAV9-TnT-*Pak3* injected mice followed by 2 weeks ISO stress, evident by 2 times higher the number of TUNEL-positive nuclei compared to the controls (Figure 3E). Therefore, the data obtained from both models reveal that PAK3 overexpression impairs adaptive cardiac autophagy, aggravating pathological stress-induced cell death and progression to heart failure.

PAK3 suppresses cardiac autophagy under starvation

The most typical trigger of autophagy is nutrient withdrawal; therefore, we employed neonatal rat cardiomyocytes (NRCMs) exposed to starvation as the *in vitro* model to confirm PAK3 regulation of autophagy. Cardiomyocytes were infected with Ad-*Pak3*-T421E, an adenovirus expressing constitutively active PAK3[37] as shown by its increased phosphorylation, or Ad-*Pak3*-T421A, overexpressing the kinase dead PAK3 Figure S4). To assess whether PAK3 blocks starvation-induced autophagy, activated PAK3-overexpressed NRCMs were starved in serum-free Earle's Balanced salt solution for 4 h. In line with the observations obtained from the *in vivo* model, starvation-induced autophagic activity was limited by PAK3 hyper-activation, as monitored by lower endogenous LC3II/I, higher p62, combined with the decreased expression of key autophagic markers, such as ULK1 and ATG5-12 (Figure 4A). In addition, the autophagic flux was impaired by PAK3 overexpression, as indicated by a decreased ratio LC3II/I and p62 during starvation when chloroquine is used to prevent the fusion of the autophagosome to the lysosome (Figure 4B). A more evident result was observed with Bafilomycin A, a different lysosomal inhibitor blocking the autophagic flux. A decreased accumulation of LC3II and p62 was detected in PAK3 overexpressed cells even without starvation (Figure S5).

More convincingly, the dynamic change of autophagic flux in H9C2 was examined with the mCherry-GFP-LC3 reporter. Free autophagosomes are visualized by overlapped GFP and mCherry fluorescent signals, whereas autolysosomes are detected by mCherry fluorescence only, because of the sensitivity of GFP to acidic conditions. As anticipated, starvation induced more autophagosomes and autolysosomes; however, PAK3 overexpression obstructed both (Figure 4C). Furthermore, the quantification of the autophagy flux reporter by flow cytometry confirmed the impairment of the starvation response (Figure 4D). Finally, aggravated cell death was observed in PAK3-overexpressed NRCMs (Figure 4E), with the increased level of released lactate dehydrogenase (LDH), an indicator of cardiomyocyte damage (Figure 4F).

On the other hand, we assessed whether PAK3 loss can preserve autophagy induced by nutrient deficiency. Autophagy declined in cardiomyocytes after prolonged starvation (Figure 4G); intriguingly, PAK3 knockdown in NRCMs using its siRNA (Figure S6) preserved autophagic activity, determined by elevated LC3, ATG5-12, and ULK1 phosphorylation at Serine 555 (Figure 4G). Also, mCherry-GFP-LC3-expressing H9C2 maintained starvation-induced autophagosomes and autolysosomes upon PAK3 disruption (Figure S7). These data further support that PAK3 overexpression impedes the autophagic process, whereas PAK3 disruption preserves autophagic activity in cardiomyocytes in response to pathological stress.

PAK3 positively regulates mTORC1

We next sought to uncover the underlying molecular mechanism through which PAK3 could regulate autophagy. First, we performed unbiased pull-down and LC/MS on PAK3-overexpressed cells under either basal conditions or starvation. Among the 287 detected proteins, 85 were found to be changed after starvation. The Reactome database and pathway analysis revealed that several pathways related to cell death were upregulated (Figure S8A). More surprisingly, an mTORC1 regulation pathway was also increased with starvation (Figure 5A), and among the PAK3 interactors, we found Folliculin, an mTORC1 promoter[38] (Figure S8B). Of note, the association of activated PAK3 with Folliculin was confirmed by co-immunoprecipitation and western blot (Figure S9A). The data suggest that during stress conditions, there is increased interaction and association between PAK3 and autophagy through mTORC1 regulation.

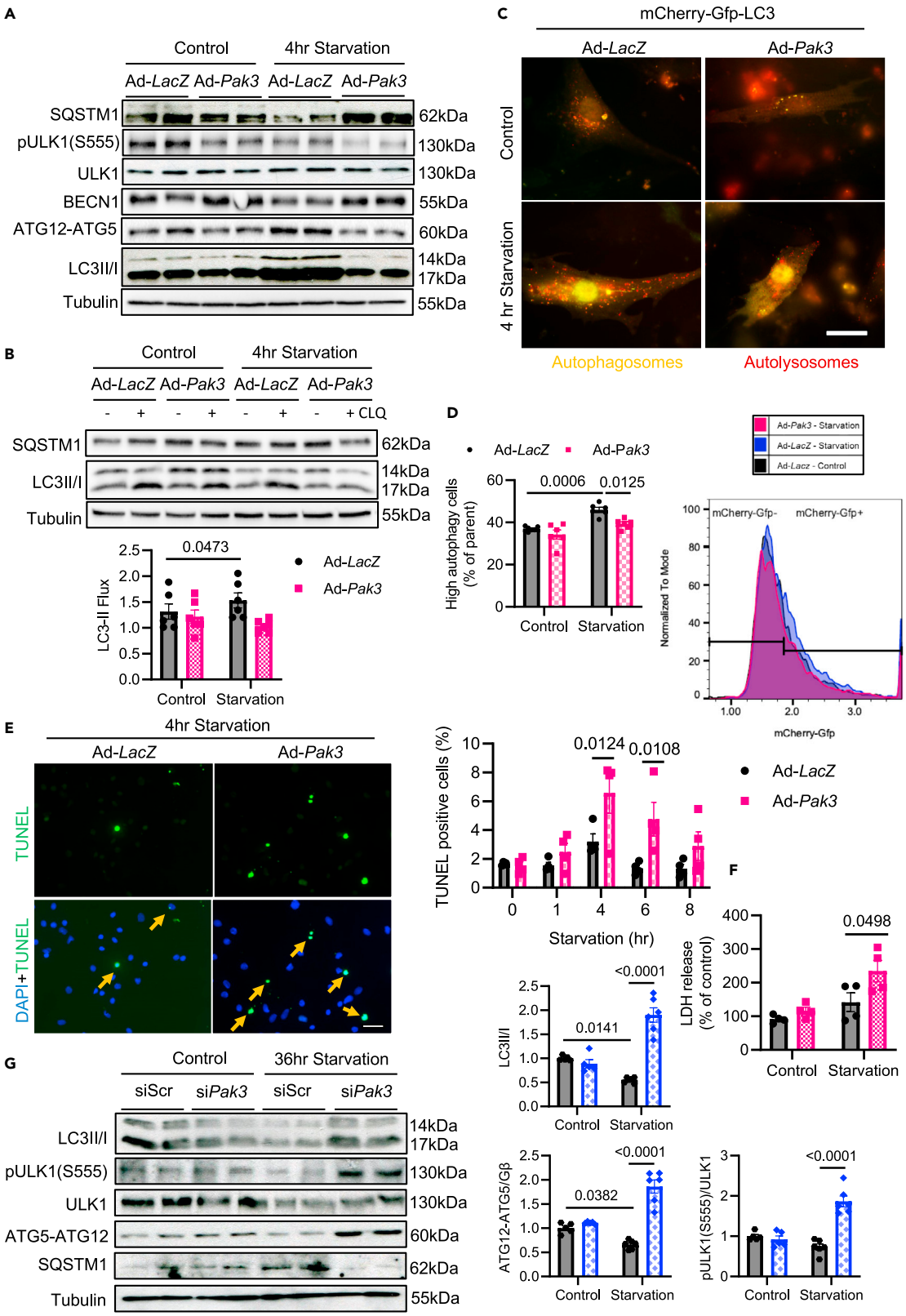
A
Control
4hr Starvation
Ad-LacZ Ad-Pak3 Ad-LacZ Ad-Pak3
SQSTM1
pULK1(S555)
ULK1
BECN1
ATG12-ATG5
LC3II/I
Tubulin
62kDa
130kDa
130kDa
55kDa
60kDa
14kDa
17kDa
55kDa
B
Control
4hr Starvation
Ad-LacZ Ad-Pak3 Ad-LacZ Ad-Pak3
- + - + - + - + CLQ
SQSTM1
LC3II/I
Tubulin
62kDa
14kDa
17kDa
55kDa
LC3-II Flux
0.0473
Ad-LacZ
Ad-Pak3
Control Starvation
C
mCherry-Gfp-LC3
Ad-LacZ
Ad-Pak3
Control
4 hr Starvation
Autophagosomes
Autolysosomes
D
Ad-LacZ
Ad-Pak3
High autophagy cells (% of parent)
0.0006
0.0125
Control Starvation
Ad-Pak3 - Starvation
Ad-LacZ - Starvation
Ad-Lacz - Control
mCherry-Gfp-
mCherry-Gfp+
Normalized To Mode
mCherry-Gfp
E
4hr Starvation
Ad-LacZ
Ad-Pak3
TUNEL
DAPI+TUNEL
TUNEL positive cells (%)
0.0124
0.0108
Ad-LacZ
Ad-Pak3
Starvation (hr)
F
LC3II/I
<0.0001
0.0141
Control Starvation
LDH release (% of control)
0.0498
Control Starvation
G
Control
36hr Starvation
siScr siPak3 siScr siPak3
LC3II/I
pULK1(S555)
ULK1
ATG5-ATG12
SQSTM1
Tubulin
14kDa
17kDa
130kDa
130kDa
60kDa
62kDa
55kDa
ATG12-ATG5/Gβ
<0.0001
0.0382
Control Starvation
pULK1(S555)/ULK1
<0.0001
Control Starvation

Figure 4. PAK3 suppresses the starvation-induced autophagic process

(A) Representative immunoblot images for autophagic markers in NRCMs exposed to 4hr-starvation.

(B) Autophagic flux was measured by immunoblots of p62 and LC3II/I in NRCMs in the presence of chloroquine (CLQ, 50μM) with 4hr-starvation. N = 6.

(C) Representative images of autophagosomes and autolysosomes in Ad-*LacZ* or Ad-*Pak3* infected H9C2 cells expressed with mCherry-Gfp-LC3 in response to 4hr-starvation. Scale bar: 20 μm.

(D) Quantification of autophagy flux in response to starvation determined by flow cytometry using the mCherry-Gfp-LC3 reporter. N = 6.

(E) TUNEL staining in control and PAK3-overexpressed NRCMs. Scale bar: 50 μm. N = 5–6.

(F) Level of lactate dehydrogenase (LDH) released from NRCMs upon starvation for 4 h. N = 4.

(G) Immunoblots and quantification of autophagic markers in PAK3-deficient NRCMs upon 36hr-starvation. N = 5–6.

Data presented as mean ± SEM. (B, F, G) Multiple comparison p values were calculated by two-way ANOVA with Tukey's or (D, E) Sidak's post hoc test.

Activation of mTORC1 is known as a major negative regulator of autophagy; therefore, we further examined whether PAK3 impairs autophagy through the modulation of mTOR activation or expression. We found mTOR activity in the myocardium was remarkably enhanced in the mice with PAK3 overexpression in the heart under either basal level or ISO stress for 2 days (Figure 5B) and 2 weeks (Figure 5C), which was determined by phosphorylation of mTOR at Serine 2448, an indication of its activation. In addition, phosphorylation of ULK1 at Serine 757 is performed by activated mTORC1, which was observed in the PAK3-overexpressed myocardium after 2-week ISO (Figures 5B and 5C). AMP-activated protein kinase (AMPK) is considered an endogenous inhibitor of mTORC1 and an autophagy activator through phosphorylation of ULK1 at Serine 555. Notably, the activation of AMPK was diminished because of PAK3 overexpression (Figures 5B and 5C), further supporting the role of PAK3 in inhibiting autophagy in the heart.

In agreement with the observations in the myocardium, NRCMs with PAK3 overexpression displayed an increase in mTOR phosphorylation but reduced AMPK activation (Figure 5D). On the contrary, PAK3 knockdown maintained the deactivation of mTOR (Figure 5E). Therefore, to further evaluate whether PAK3 blockage of autophagy is mTORC1 dependent, NRCMs were pre-treated with the well-known mTORC1 inhibitor, rapamycin. Noticeably, the addition of rapamycin before starvation preserved LC3II/I ratio in PAK3-overexpressed NRCMs (Figure 5F). Whereas, AICAR, an AMPK activator, failed to rescue PAK3-suppressed autophagy under starvation (Figure 5G). Moreover, in response to ISO stimulation, phosphorylation of mTOR was also augmented by activated PAK3, but not affected by the kinase-dead PAK3 (Figure S9B), indicating PAK3 action on mTOR was kinase activity-dependent. The above data demonstrate that pathological stress-induced PAK3 restrains cardiac autophagy, likely through hyper-activation of mTORC1.

PAK3 overexpression constrains autophagy in human cardiac tissue and cells

We obtained human-relevant evidence of PAK3 negatively regulating autophagy in the heart under pathological stress from cultured human heart slices infected with Ad-*Pak3*-T421E (Figure S10), followed by ISO stimulation for 1 h. Of interest, we found that PAK3 led to a higher level of mTOR phosphorylation at Serine 2448 in both control and starved conditions (Figure 6A). PAK3-overexpression lessened LC3II/I ratio and ATG5-12, but augmented p62 accumulation, suggesting a blockage of the autophagic process (Figure 6A). Furthermore, the cultured human heart slices with PAK3 overexpression were co-treated with ISO and chloroquine to assess the role of PAK3 in autophagic flux. Chloroquine induced a clear increase in LC3II/I ratio, with an analogous accumulation of p62 in the control group in the presence of ISO (Figure 6B); however, PAK3 overexpression ablated such response, indicating PAK3 repression of autophagic flux (Figure 6B).

In addition, human induced pluripotent stem cell-derived cardiomyocytes (iPSC-CMs) (Figure S11) with PAK3 overexpression failed to display the starvation-induced endogenous LC3 dot formation (Figure 6C). Moreover, more apoptosis (Figure 6D) and protein aggregation (Figure 6E) were found in PAK3-overexpressed iPSC-CMs. These data support that PAK3 blunts stress-induced autophagy in human-relevant models.

Pharmacological preservation of autophagy ameliorates PAK3-induced cardiac dysfunction

Finally, we gathered functional evidence on the feasibility of preserving cardiac autophagy and function despite PAK3 upregulation under pathological stress. A recently identified autophagy enhancer, MSL-7, activates autophagy by enhancing transcription factor EB (TFEB), a major regulator that promotes lysosomal biogenesis and the autophagic process.[39,40] Prompted by our observations that cardiac PAK3 upregulation is associated with the repression of autophagy and the resultant cardiac dysfunction, we used MSL-7 to assess whether preserving cardiac autophagy has beneficial effects on cardiac hypertrophy and heart failure in the face of pathological stress. First, we validated MSL-7's role in cardiac autophagy

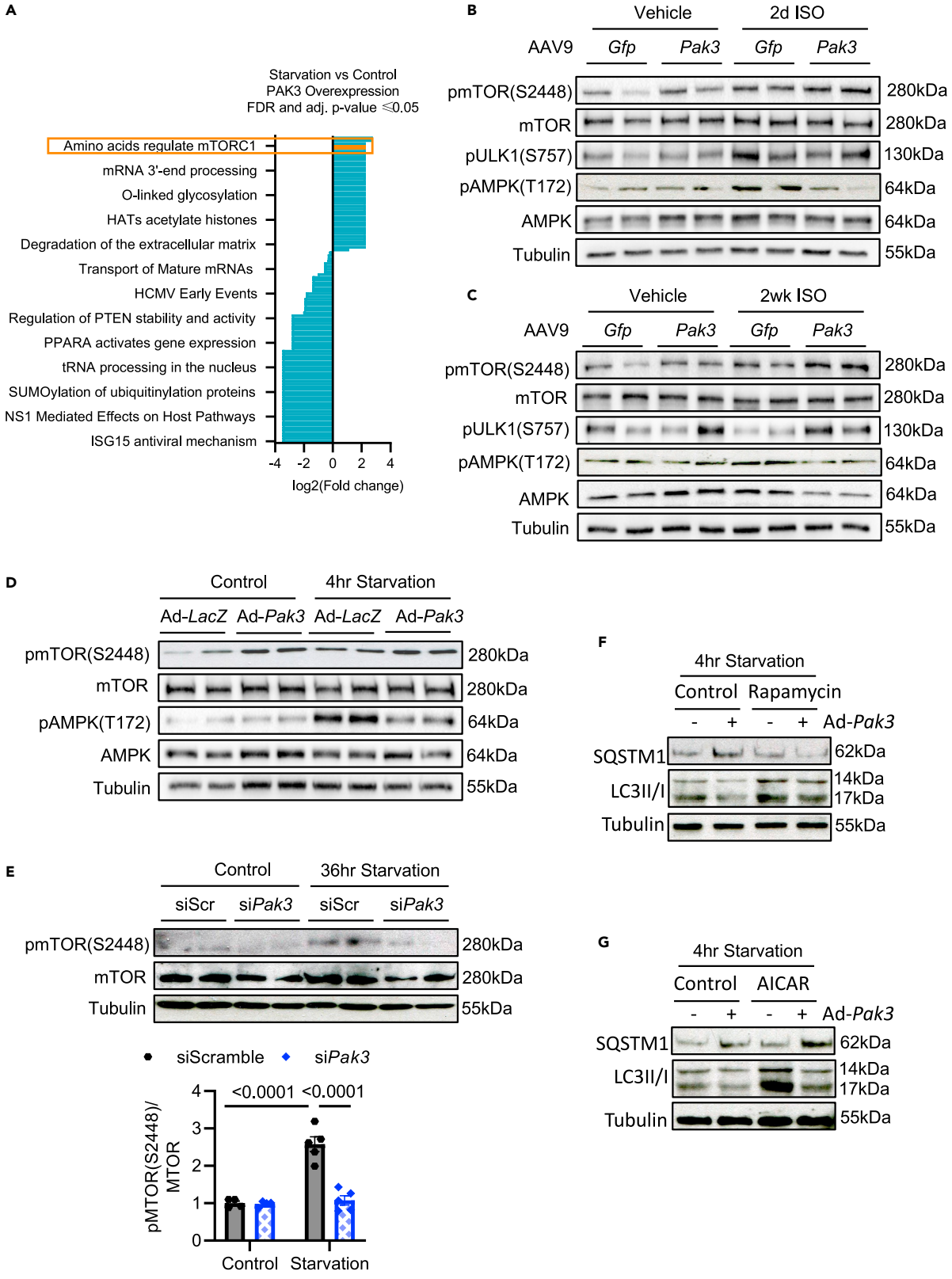
A
Starvation vs Control
PAK3 Overexpression
FDR and adj. p-value ⩽0.05
Amino acids regulate mTORC1
mRNA 3'-end processing
O-linked glycosylation
HATs acetylate histones
Degradation of the extracellular matrix
Transport of Mature mRNAs
HCMV Early Events
Regulation of PTEN stability and activity
PPARA activates gene expression
tRNA processing in the nucleus
SUMOylation of ubiquitinylation proteins
NS1 Mediated Effects on Host Pathways
ISG15 antiviral mechanism
-4 -2 0 2 4
log2(Fold change)
B
Vehicle
2d ISO
AAV9 Gfp Pak3 Gfp Pak3
pmTOR(S2448) 280kDa
mTOR 280kDa
pULK1(S757) 130kDa
pAMPK(T172) 64kDa
AMPK 64kDa
Tubulin 55kDa
C
Vehicle
2wk ISO
AAV9 Gfp Pak3 Gfp Pak3
pmTOR(S2448) 280kDa
mTOR 280kDa
pULK1(S757) 130kDa
pAMPK(T172) 64kDa
AMPK 64kDa
Tubulin 55kDa
D
Control
4hr Starvation
Ad-LacZ Ad-Pak3 Ad-LacZ Ad-Pak3
pmTOR(S2448) 280kDa
mTOR 280kDa
pAMPK(T172) 64kDa
AMPK 64kDa
Tubulin 55kDa
E
Control
36hr Starvation
siScr siPak3 siScr siPak3
pmTOR(S2448) 280kDa
mTOR 280kDa
Tubulin 55kDa
siScramble
siPak3
<0.0001 <0.0001
pMTOR(S2448)/ MTOR
0 1 2 3 4
Control Starvation
F
4hr Starvation
Control Rapamycin
- + - + Ad-Pak3
SQSTM1 62kDa
LC3II/I 14kDa 17kDa
Tubulin 55kDa
G
4hr Starvation
Control AICAR
- + - + Ad-Pak3
SQSTM1 62kDa
LC3II/I 14kDa 17kDa
Tubulin 55kDa

Figure 5. PAK3 positively regulates mTOR activity

(A) Reactome pathway analysis of potential PAK3 interactors under starvation stimulation. Flag-*Pak3* complexes were immunoprecipitated with FLAG antibody and identified by LC-MS/MS. A sample without overexpression was used as a negative control to eliminate proteins trapped by unspecific binding. Pathways with both FDR and Adj. P-value lower than 0.05 were selected. The graph shows the fold change of key pathways changed upon stimulation.

(B and C) Immunoblots of mTOR, ULK1, and AMPK in the heart of mice 2-day (B) or 2 weeks post-ISO stress (C).

(D–G) Immunoblots on PAK3 overexpressed-NRCMs (D) or PAK3 knockdown (siRNA)-NRCMs (E). Representative images for p62 (SQSTM1) and LC3 in PAK3-overexpressed (Ad-*Pak3*) NRCMs pre-treated with rapamycin (mTOR1 inhibitor, 5μM) (F) or AICAR (AMPK activator, 1mM) (G). N = 5–6.

Data presented as mean ± SEM. p values vs. control were determined by (A) two-tailed Student's *t-test* adjusted with False Discovery Rate, and (E) multiple comparison p values were calculated by two-way ANOVA with Tukey's correction.

activation. Although MSL-7 did not affect PAK3 and mTOR expression in cultured cardiomyocytes, its higher doses increased ULK1 expression (Figure S12A). It should be mentioned that the *in vitro* screening was not designed with equal serial dilutions but following the observations of previous studies.[39,40] More importantly, the preliminary functional evidence from cardiac-specific PAK3-overexpressed mice administered two doses of intraperitoneal injection of MSL-7 showed its capacity to maintain cardiac function under ISO stress (Figure S12B; Table S3).

In subsequent experiments, the mice with cardiac PAK3 overexpression were subjected to constant ISO stimulation, accompanied by intraperitoneal injection of MSL-7 thrice weekly (Figure 7A). After 2 weeks, compared to the untreated group, PAK3-overexpressed hearts receiving MSL-7 treatment displayed an improved cardiac performance and reduced dilation, as indicated by rescued FS% and smaller ventricular chamber (Figure 7B; Table S4). Assessment of the thickness of the posterior wall demonstrated a compensated hypertrophic remodeling by MSL-7, albeit heart weight showing only a trend toward an increase in comparison to the untreated group (Figure 7C; Table S4). At the cellular level, the cross-sectional area was increased by MSL-7 treatment (Figure 7D); however, the treatment prevented interstitial fibrosis and cardiomyocyte death, despite PAK3-overexpression (Figures 7E and 7F), suggesting that MSL-7 can prevent pathological cardiac dilation and heart failure. Concomitantly, the impairment of autophagy in PAK3-overexpressed myocardium was prevented by MSL-7 treatment after 2-week ISO stimulation, marked by higher LC3II/I ratio, ATG5-12, and phosphorylation ULK1 (S555) with lower p62 aggregation under ISO stress, likely because of enhanced TFEB-induced lysosomal and autophagic actions (Figure 7G), indicating that MSL-7 is able to fulfill its protective action on cardiac function via proper autophagic response. These results provide insights into the importance and feasibility of maintaining adaptive autophagy in the heart to prevent pathological stress-induced heart failure.

DISCUSSION

Multiple factors contribute to the onset and progression of cardiac dysfunction in response to pathological stress. Autophagy in cardiomyocytes is a fine-tuned mechanism to govern protein and organelle turnover; thus, its defects damage cellular homeostasis. Led by consistent observation of increased PAK3 in the failing hearts, this study has also demonstrated: (1) overexpression of PAK3 in cardiomyocytes made the heart more susceptible to cardiac remodeling and dysfunction on pathological stress; (2) PAK3 suppressed adaptive autophagy likely through hyper-activation of mTORC1, consequently leading to more cell death; (3) the treatment by an autophagic enhancer, MSL-7, prevented PAK3-triggered defective autophagy and preserved cardiac function under isoprenaline stimulation. Our data provide new insights into the clinical implications of treating heart failure by preserving the cardiac autophagic process.

PAK3 overexpression causes heart failure

Considering the biological roles of PAKs in various cell types, their abnormal activation is associated with inflammation, neurological disorders, metabolic disorders, and infectious diseases. In group I PAKs, PAK1, PAK2, and PAK3 play biological roles via similar mechanisms.[41] Although PAK1 and PAK2 have been well studied, studies on PAK3 are underway. For instance, PAK3 mutations are implicated in mental retardation or intellectual disability.[42,43] PAK3 is also required for actin organization and migration in fibroblasts,[44] whereas it is responsible for glioblastoma migration and invasion.[45]

In the myocardium, contrary to the antihypertrophic roles of PAK1 and PAK2, an abstract reported that PAK3 loss attenuates cardiac pathological hypertrophy.[46] Upregulated PAK3 and its phosphorylation in the failing heart made us speculate on the relevance between PAK3 and the development of heart failure. Mice with cardiac PAK3 overexpression did not present any cardiac remodeling under unstressed conditions, but they failed to develop compensated hypertrophy in response to pathological stress.

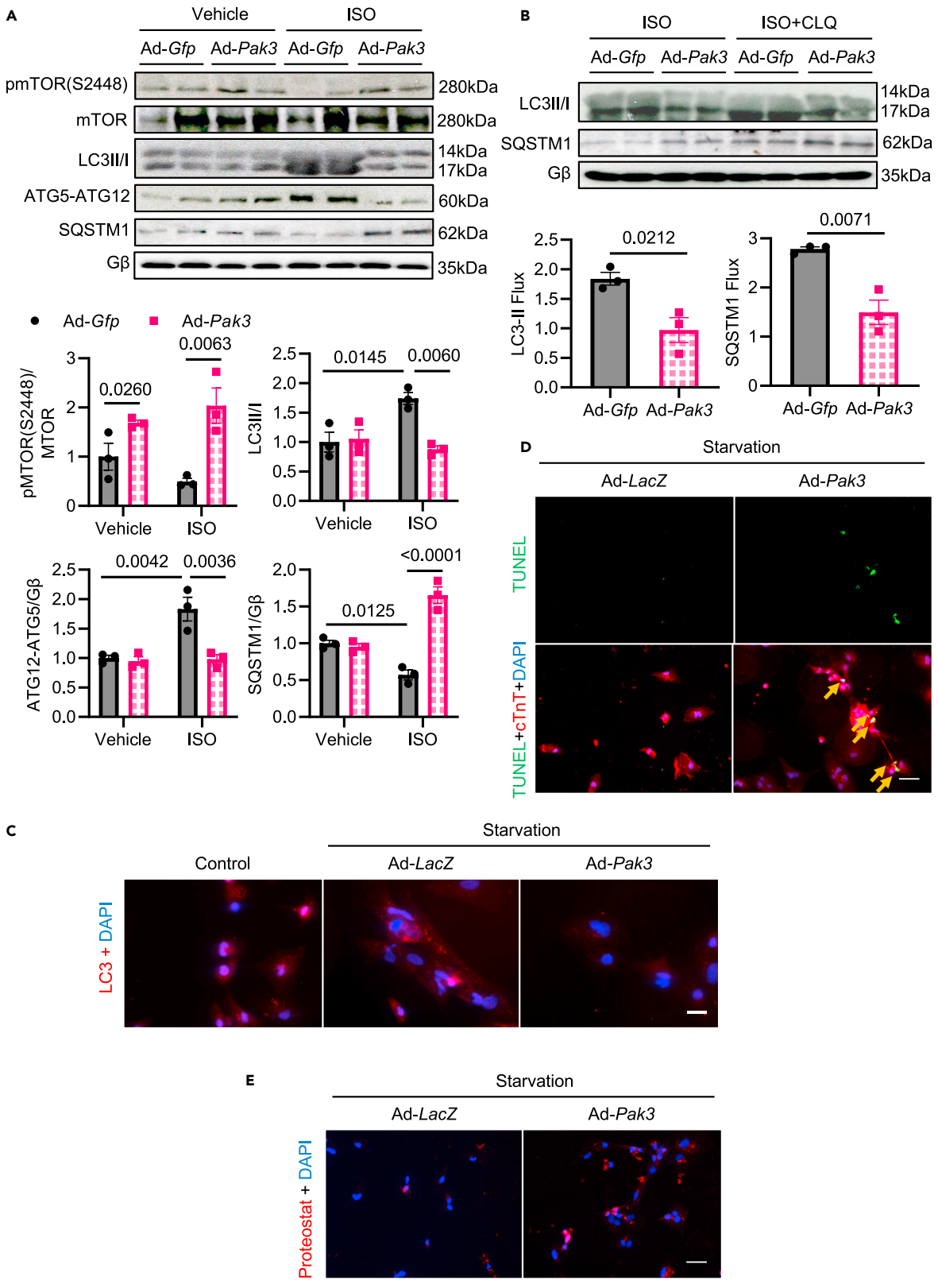
A
Vehicle
ISO
Ad-Gfp
Ad-Pak3
Ad-Gfp
Ad-Pak3
pmTOR(S2448)
mTOR
LC3II/I
ATG5-ATG12
SQSTM1
Gβ
280kDa
280kDa
14kDa
17kDa
60kDa
62kDa
35kDa
Ad-Gfp
Ad-Pak3
pMTOR(S2448)/MTOR
0.0260
0.0063
Vehicle
ISO
LC3II/I
0.0145
0.0060
Vehicle
ISO
ATG12-ATG5/Gβ
0.0042
0.0036
Vehicle
ISO
SQSTM1/Gβ
0.0125
<0.0001
Vehicle
ISO
B
ISO
ISO+CLQ
Ad-Gfp
Ad-Pak3
Ad-Gfp
Ad-Pak3
LC3II/I
SQSTM1
Gβ
14kDa
17kDa
62kDa
35kDa
LC3-II Flux
0.0212
Ad-Gfp
Ad-Pak3
SQSTM1 Flux
0.0071
Ad-Gfp
Ad-Pak3
C
Starvation
Control
Ad-LacZ
Ad-Pak3
LC3 + DAPI
D
Starvation
Ad-LacZ
Ad-Pak3
TUNEL
TUNEL+cTnT+DAPI
E
Starvation
Ad-LacZ
Ad-Pak3
Proteostat + DAPI

Figure 6. Human evidence for PAK3 inhibition of autophagy via mTOR activation

(A and B) (A) Immunoblots and quantification graphs of autophagic markers in cultured human heart slices overexpressing PAK3 under 1hr-ISO (10μM) stimulation. (B) Autophagic flux was measured by immunoblots of LC3 and p62 (SQSTM1) in the presence of chloroquine treatment (50μM). N = 3.
(C–E) (C) Immunofluorescence for LC3 on PAK3 overexpressed human induced pluripotent stem cell-derived cardiomyocytes (iPSC-CMs) following 4-h starvation. Scale bar: 50 μm. (D) TUNEL staining (scale bar: 50μm) for apoptosis detection and (E) protein aggregation (scale bar: 20μm) assessed by Proteostat staining on iPSC-CMs.

Data presented as mean ± SEM. p values vs. control were determined by (B) two-tailed unpaired Student's *t-test*, and (A) multiple comparison p values were calculated by two-way ANOVA with Tukey's correction.

Consequently, the mice were vulnerable to heart failure in response to pathological stress, evidenced by increased fibrosis, apparent apoptosis, and elevated *Nppb*, a biomarker of heart failure. Noticeably, the PAK3-overexpressed heart manifested declined systolic function on acute ISO stimulation, indicating that PAK3 overexpression makes the heart less resistant to stress. Thus, our study proposed that PAK3 contributes to heart failure progression. More importantly, most PAKs have oncogenic impacts; therefore, preventing heart failure by targeting PAK3 may avoid triggering cancer development. Discovery and further investigation of PAK3-specific inhibitors as a possible treatment will be carried on in the subsequent studies.

PAK3 represses adaptive cardiac autophagy

In the heart, proper and dynamic autophagic activity is essential for maintaining cardiomyocyte homeostasis, whereas autophagy perturbation contributes to the progression of heart failure.[5–7,10–12] Particularly, excessive levels of autophagy promote cell death by activating apoptotic mechanisms; for instance, ATG5-12 can trigger caspase activation.[6,12] PAK3 overexpression led to blocked autophagy, as assessed by autophagic markers in gain-of-function *in vivo* and *in vitro* models, such as LC3II/I ratio, ATG5-12, and ULK1. A decrease in these indicators of autophagosome formation suggested that PAK3 blocks autophagic initiation in the heart facing acute stress, while increased p62 in PAK3-overexpression on stress implied that PAK3 impairs the autophagic process. In addition, autophagic flux was hindered by PAK3 overexpression, indicated by a lower rate of LC3 and p62 accumulation under chloroquine incubation. Notably, cultured human heart slices with PAK3 overexpression failed to display adaptive autophagic activity induced by acute ISO. Akin to the observations on ISO stress, PAK3 overexpression blunted LC3 dots in iPSC-CMs under starvation, associated with apparent protein aggregation and apoptosis. All data suggested that PAK3 interferes with the autophagic process, and this role is conserved in mouse, rat, and human models.

Strikingly, PAK3 overexpression did not affect autophagic events in basal conditions, and there were comparable levels of autophagosomes and autolysosomes in PAK3-knockdown NRCMs compared to wild-type cells during long-term stress. These observations underlined that PAK3 upregulation is sufficient to repress adaptive autophagy when facing pathological stress and that targeting PAK3 can maintain proper rather than trigger excessive autophagy.

PAK3 promotes the activation of mTORC1

The mTORC1 complex is formed by three core components: mTOR, Raptor, and mLST8. Activated mTORC1 restrains autophagy. For example, mTORC1 inhibits autophagosome initiation primed by ULK1 and deters autophagosome maturation by downregulating TFEB-regulated genes.[19,20] Unbiased MS analyses disclosed a potential interaction between PAK3 and mTOR regulation. We found that PAK3 overexpression increased mTOR phosphorylation under both stressed and unstressed conditions, albeit an unchanged expression of mTOR. Particularly, only activated PAK3 overexpression augmented phosphorylation of mTOR; whereas overexpression of kinase-dead PAK3 did not affect mTOR activity. In addition, activated PAK3 interacted with Folliculin, which can mediate mTOR phosphorylation.[38] In addition, PAK3 activity also increased Folliculin expression; however, the mechanisms will be investigated in depth in the future. Rapamycin is a selective inhibitor of mTORC1; therefore, it is considered an autophagic inducer by suppressing mTOR.[47] Of interest, PAK3 overexpression failed to block rapamycin-induced autophagy, indicating that the effect of PAK3 on autophagy is mTORC1-dependent, probably by mTORC1 downregulation of TFEB.[19,20]

An accelerated rate of global protein synthesis is a crucial feature of cardiomyocyte hypertrophy, associated with increased translational efficiency and translational capacity.[1] In addition to repression

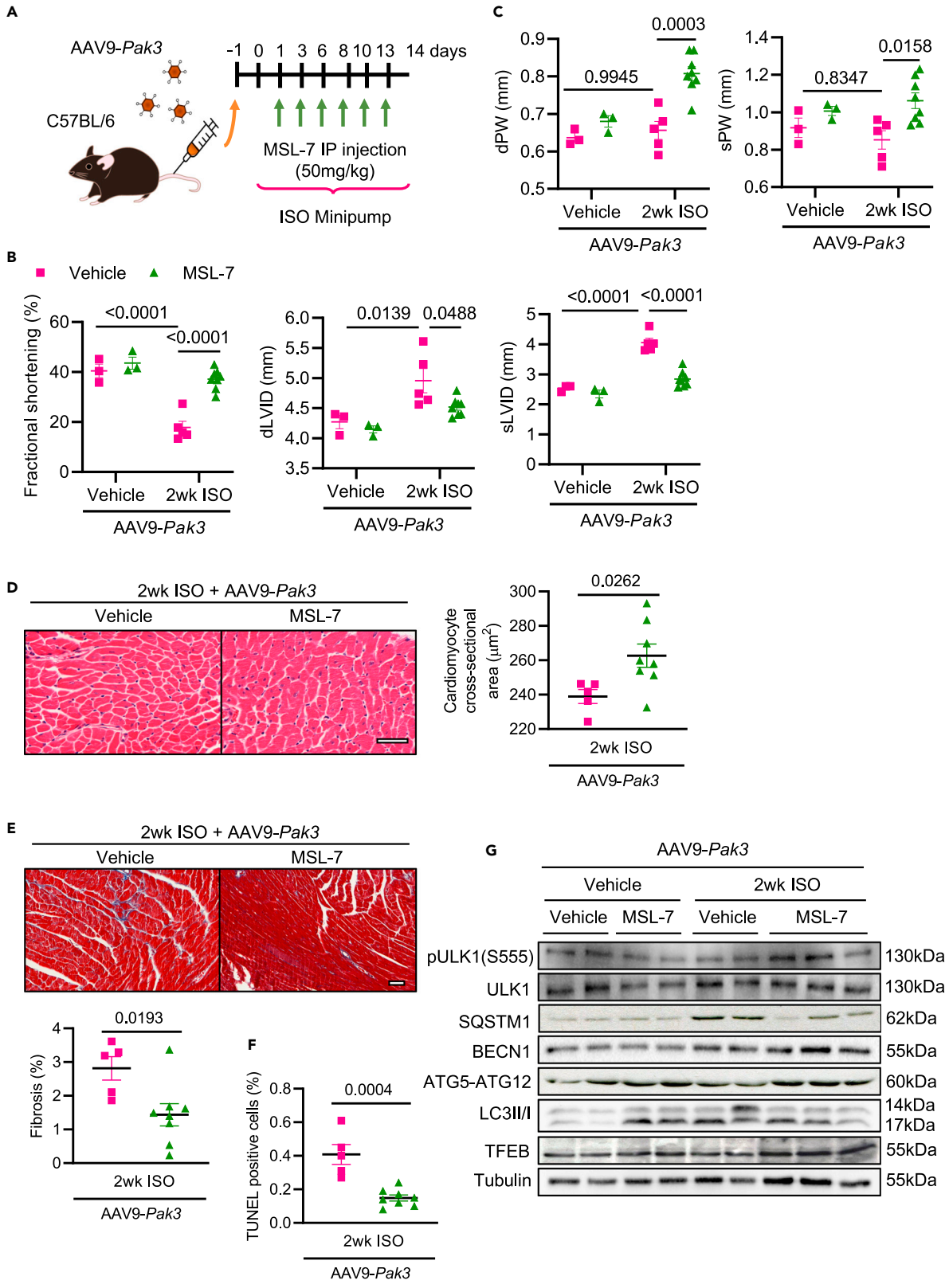
A
AAV9-Pak3
-1 0 1 3 6 8 10 13 14 days
C57BL/6
MSL-7 IP injection
(50mg/kg)
ISO Minipump
C
dPW (mm)
0.9945
0.0003
Vehicle
2wk ISO
AAV9-Pak3
sPW (mm)
0.8347
0.0158
Vehicle
2wk ISO
AAV9-Pak3
B
Vehicle
MSL-7
Fractional shortening (%)
<0.0001
<0.0001
Vehicle
2wk ISO
AAV9-Pak3
dLVID (mm)
0.0139
0.0488
Vehicle
2wk ISO
AAV9-Pak3
sLVID (mm)
<0.0001
<0.0001
Vehicle
2wk ISO
AAV9-Pak3
D
2wk ISO + AAV9-Pak3
Vehicle
MSL-7
Cardiomyocyte cross-sectional area (μm2)
0.0262
2wk ISO
AAV9-Pak3
E
2wk ISO + AAV9-Pak3
Vehicle
MSL-7
Fibrosis (%)
0.0193
2wk ISO
AAV9-Pak3
F
TUNEL positive cells (%)
0.0004
2wk ISO
AAV9-Pak3
G
AAV9-Pak3
Vehicle
2wk ISO
Vehicle
MSL-7
Vehicle
MSL-7
pULK1(S555)
ULK1
SQSTM1
BECN1
ATG5-ATG12
LC3II/I
TFEB
Tubulin
130kDa
130kDa
62kDa
55kDa
60kDa
14kDa
17kDa
55kDa
55kDa

Figure 7. An autophagy inducer prevents the detrimental effects of PAK3 overexpression in cardiac function

(A) Schematic figure of the experiment by constant ISO infusion accompanied by MSL-7 IP injection every three days for two weeks (50 mg/kg).

(B and C) (B) Fractional shortening (%), end-diastolic left ventricular internal diameter (dLVID), sLVID, (C) dPW and end-systolic left ventricular posterior wall thickness (sPW) in PAK3-overexpressed hearts receiving MSL-7 treatment or vehicle following ISO stimulation. N = 3–8.

(D and E) H&E staining images of average cross-sectional area (D), and interstitial fibrosis detected by Masson's Trichrome staining (E) in the heart. Scale bar: 50 μm. N = 5–8.

(F) Quantification of TUNEL-positive cells for detection of apoptosis. N = 6–8.

(G) Representative immunoblots of autophagic markers from the heart extracts.

Data presented as mean ± SEM. p values vs. control were determined by (D, E, F) two-tailed unpaired Student's *t-test*, and (B, C) multiple comparison p values were calculated by two-way ANOVA with Tukey's correction.

of autophagy, mTOR is known to promote ribosomal biogenesis and protein translation through activation of the substrates, ribosomal protein S6 protein kinase 1 (S6K1), and eukaryotic translation initiation factor 4E-binding protein 1 (4E-BP1).[48] Activation of mTOR and S6K1 has been implicated in triggering cardiac hypertrophy, whereas ablation of mTOR and 4E-BP1 impair hypertrophic response under pressure overload stress.[26] In addition, rapamycin is able to revert the established cardiac hypertrophy.[23] We demonstrated that hearts with PAK3 overexpression displayed enlarged cardiomyocytes in long-term ISO stimulation, despite unaltered cell growth under either un-stressed or acute stressed conditions. However, it is unclear whether PAK3-induced cell growth is a consequence of mTOR-enhanced protein synthesis. The current study did not investigate the mechanistic link between PAK3 regulation of autophagy and cardiac pathological hypertrophy, which will be further explored.

Regulation of mTORC1 in the myocardium

Turnover of amino acids achieved by autophagy may be an essential source of energy for cardiomyocyte survival during pathological stressed conditions. Cardiomyocytes are sensitive to nutrient deficiency, which induces autophagy via the AMPK energy-sensing pathway. AMPK's action on autophagy is, at least in part, through phosphorylation of ULK1 at multiple sites, including Serine 555.[19] However, mTORC1 phosphorylation of Serine 757 in ULK1 disrupts its interaction with AMPK, blocking the autophagy-initiating complex.[19] We detected a decreased AMPK activation because of PAK3 overexpression under stressed conditions, which could explain the decreased phosphorylation of ULK1 at Serine 555. However, the observation that the AMPK activator, AICAR, could not induce autophagy in PAK3-overexpressed cells indicated that negative regulation of PAK3 on autophagy is not directly through suppression of AMPK.

In addition, activated AMPK inhibits mTORC1 signaling by phosphorylation of Tuberous sclerosis complex 2 (TSC2), which blocks mTORC1 association with its activator Rheb-GTP.[49] In the heart, loss of TSC2 downregulates autophagy and induces cardiac dysfunction,[27,50] whereas increased TSC2 is sufficient to reduce cardiac hypertrophic growth.[24] On the other hand, mTORC1 can downregulate AMPK by phosphorylating its Serine 367,[51] which may explain the observations of PAK3 overexpression-repressed AMPK phosphorylation. As such, future study is needed to decipher the mechanisms underlying PAK3 regulation of mTORC1 and AMPK in the myocardium.

Limitations of treatment by modulating mTORC1 pathway

In pre-clinical studies, inhibition of mTORC1 by rapamycin successfully delays the onset of age-related diseases, including cancer, neurodegenerative diseases, age-related diseases, and cardiovascular diseases.[52,53] However, clinical usage of rapamycin and its analogs are associated with some side effects, limiting their potential and safety for long-term use. The side effects include an increased risk of type 2 diabetes, thrombocytopenia, hyperlipidemia, immunosuppression, and nephrotoxicity.[53] For instance, the FDA-approved rapalogs (sirolimus, everolimus, and temsirolimus) give rise to impaired insulin sensitivity and anomalous immune cell profile in mice.[54] More importantly, according to the action of mTORC1 on promoting protein synthesis and inhibiting autophagy, mTORC1 is required for cardiac development and adaptive hypertrophic response, whereas pharmacological blockade of mTORC1 activation confers cardioprotection.[22] Our study provides insights into a new regulator of mTORC1 and the possibility of targeting it in the future, perhaps with reduced side effects than those observed by direct mTORC1 modulation.

Treatment potential of restoration of cardiac autophagy under stress

As aforementioned, despite the advances in clinical treatment approaches for heart failure, morbidity and mortality remain high. Developing better and more targeted therapeutic strategies to prevent or treat heart failure is urgently needed. MSL-7 is a small molecule recently identified to enhance autophagy.[39,40] Although

MSL-7 does not inhibit mTORC1 activity, it induces calcineurin dephosphorylation of TFEB in HeLa cells and β-cells.[39,40] Subsequently, nuclear translocation of TFEB upregulates genes participating in lysosomal biogenesis and autophagy.[55] *In vivo*, MSL-7 administration boosted autophagy, improved glucose and lipid metabolism, and attenuated inflammation in obese and diabetic mice.[39] In addition, this autophagy enhancer showed the therapeutic potential of improving glucose tolerance and β-cell function by promoting clearance of islet amyloid accumulation.[40] However, the effects of MSL-7 on cardiac function had never been assessed. Following previous studies,[39] we tested two working concentrations of MSL-7 on mice and selected the lower dose, which showed similar functional effects to the higher one, for our experiments. We demonstrated that MSL-7 administration mitigated PAK3 overexpression-induced cardiac dysfunction in mice under ISO stimulation. Consistent with its molecular action reported previously, MSL-7 augmented autophagic markers associated with higher TFEB in the myocardium, albeit PAK3 overexpression. These observations indicate that MSL-7 cardiac protective function is through a mTORC1-independent pathway.

MSL-7 also activates calcineurin in HeLa cells.[39] Calcineurin, as a Ca^{2+}-dependent phosphatase, promotes cardiac hypertrophy, at least partially, by activating NFAT transcriptional upregulation of hypertrophic genes.[16] MSL-7 treatment increased ventricular wall thickness and improved cardiac function, which is considered compensated hypertrophy. Consistent with a more significant increment in cardiomyocyte size in the MSL-7-treated group than the one observed within the PAK3 overexpression with ISO stress. More importantly, MSL-7 reduced fibrosis and apoptosis. Therefore, it is a promising candidate to treat diseases caused by defects in intracellular protein homeostasis. However, because excessive autophagy may be harmful to cells, although MSL-7 treatment within 2 weeks displayed its beneficial effects on the heart, its consequences over prolonged administration need to be carefully evaluated in the future.

Conclusion

Our study here presents, for the first time, *in vivo* evidence of PAK3 regulating autophagy in the myocardium in response to pathological stress. It also identifies PAK3 as a new regulator of the mTORC1 pathway. Furthermore, our findings offer a promising therapeutic approach for heart failure by maintaining appropriate cardiac autophagy. It is worth investigating whether PAK3 is a potential target for drug discovery in treating heart diseases with fewer side effects.

Limitations of the study

The current study demonstrates that cardiac PAK3 was upregulated in response to pathological stresses, contributing to cardiac dysfunction, at least partially, via inhibition of proper autophagic regulation in cardiomyocytes. However, there was lack of observations of cardiac PAK3 expression in human tissue at the different stages of disease. Although *in vivo* and *in vitro* models indicate that cardiomyocytes with PAK3 overexpression promoted cardiac death, more clinical evidence is needed to confirm the role of PAK3 on cardiac dysfunction. Moreover, more research on the molecular mechanisms at work are required to fully understand the role of PAK3. For instance, the pathway leading to PAK3 upregulation on pathological stress was not investigated. In addition, PAK3 inhibition of autophagy was found to be through the modulation of mTOR; however, this could be corroborated in both gain-of-function and loss-of-function mouse models under various stress periods. Further investigations are required to determine the role of PAK3 in different mTOR functions, such as protein synthesis. At the same time, even though our data show that AMPK phosphorylation was blunted by PAK3 overexpression, the association of PAK3 and AMPK was not studied in-depth. Finally, MSL-7 injections on mice showed its beneficial effects on cardiac function by rescuing autophagy, indicating it could be worthwhile investigating its efficiency on other disease and large animal models with autophagic dysfunction to determine the feasibility of employing it to prevent heart failure.

STAR★METHODS

Detailed methods are provided in the online version of this paper and include the following:

- KEY RESOURCES TABLE
- RESOURCE AVAILABILITY
  - Lead contact
  - Materials availability
  - Data and code availability
- EXPERIMENTAL MODEL AND SUBJECT DETAILS
  - Human heart protein extracts

SUPPLEMENTAL INFORMATION

Supplemental information can be found online at https://doi.org/10.1016/j.isci.2023.106970.

ACKNOWLEDGMENTS

This work was supported by the British Heart Foundation (FS/15/16/31477, FS/18/73/33973, FS/19/70/34650 and PG/19/66/34600 to W. Liu, and BHF Accelerator award AA/18/4/34221 to University of Manchester), and a professorship from the German Centre for Cardiovascular Research (81Z0700201 to O. J. Müller). T.M.A.M. is supported by NIH grants R01HL147921 and P30GM127607, U.S.A. Department of Defense grant W81XWH-20-1-0419 and American Heart Association grant 16SDG29950012. The authors also acknowledge NIH grants F32HL149140 (R.R.E.A.).

The authors wish to thank Roger Meadows, Steven Marsden, Peter March, and Darren Thomson (Bioimaging facility, University of Manchester) for technical training on microscopes; in addition to Emma-Jayne Keevil, Julian Selley, and Ronan O'Cualain (Mass spectrometry Facility, University of Manchester) for processing samples and the training on sample preparation and data analysis. We also thank Andy Hayes (Genomic technologies facility) and Ian Donaldson (Bioinformatics facility, University of Manchester) for technical support on RNA Sequencing performance and data analyses.

The Histology Facility equipment used in this study was purchased with grants from The University of Manchester Strategic Fund.

AUTHOR CONTRIBUTIONS

A.R.V. designed and carried out experiments, analyzed and interpreted data and drafted the manuscript. R.R., H.G., N.K., N.A., X.C., and O.F. acquired various data. J.M.M., R.R.E.A., Q.O., and T.M.A.M. cultured and treated human heart slices. S.H., N.F., and O.M. produced portion of AAV9-*Pak3*. X.Z. and T.W. provided technical support for iPSC experiments. X.W. reviewed study design. E.J.C. designed animal works

and reviewed the study. W.L. conceptualized the project, designed experiments, interpreted results, and drafted the manuscript.

DECLARATION OF INTERESTS

T.M.A.M. holds equities at Tenaya Therapeutics. The other authors have declared that no conflict of interest exists.

INCLUSION AND DIVERSITY

We support inclusive, diverse, and equitable conduct of research.

Received: February 1, 2023
Revised: March 27, 2023
Accepted: May 23, 2023
Published: May 26, 2023

REFERENCES

1. Simpson, L.J., Reader, J.S., and Tzima, E. (2020). Mechanical regulation of protein translation in the cardiovascular system. Front. Cell Dev. Biol. *8*, 34.

2. Lee, E., Koo, Y., Ng, A., Wei, Y., Luby-Phelps, K., Juraszek, A., Xavier, R.J., Cleaver, O., Levine, B., and Amatruda, J.F. (2014). Autophagy is essential for cardiac morphogenesis during vertebrate development. Autophagy *10*, 572–587.

3. Levine, B., and Klionsky, D.J. (2004). Development by self-digestion: molecular mechanisms and biological functions of autophagy. Dev. Cell *6*, 463–477.

4. Klionsky, D.J., and Emr, S.D. (2000). Autophagy as a regulated pathway of cellular degradation. Science *290*, 1717–1721.

5. Lavandero, S., Chiong, M., Rothermel, B.A., and Hill, J.A. (2015). Autophagy in cardiovascular biology. J. Clin. Invest. *125*, 55–64.

6. Schiattarella, G.G., and Hill, J.A. (2016). Therapeutic targeting of autophagy in cardiovascular disease. J. Mol. Cell. Cardiol. *95*, 86–93.

7. Bravo-San Pedro, J.M., Kroemer, G., and Galluzzi, L. (2017). Autophagy and mitophagy in cardiovascular disease. Circ. Res. *120*, 1812–1824.

8. Xie, M., Cho, G.W., Kong, Y., Li, D.L., Altamirano, F., Luo, X., Morales, C.R., Jiang, N., Schiattarella, G.G., May, H.I., et al. (2021). Activation of autophagic flux blunts cardiac ischemia/reperfusion injury. Circ. Res. *129*, 435–450.

9. Gu, S., Tan, J., Li, Q., Liu, S., Ma, J., Zheng, Y., Liu, J., Bi, W., Sha, P., Li, X., et al. (2020). Downregulation of LAPTM4B contributes to the impairment of the autophagic flux via unopposed activation of mTORC1 signaling during myocardial ischemia/reperfusion injury. Circ. Res. *127*, e148–e165.

10. Zhu, H., Tannous, P., Johnstone, J.L., Kong, Y., Shelton, J.M., Richardson, J.A., Le, V., Levine, B., Rothermel, B.A., and Hill, J.A. (2007). Cardiac autophagy is a maladaptive response to hemodynamic stress. J. Clin. Invest. *117*, 1782–1793.

11. Shimomura, H., Terasaki, F., Hayashi, T., Kitaura, Y., Isomura, T., and Suma, H. (2001). Autophagic degeneration as a possible mechanism of myocardial cell death in dilated cardiomyopathy. Jpn. Circ. J. *65*, 965–968.

12. Kostin, S., Pool, L., Elsässer, A., Hein, S., Drexler, H.C.A., Arnon, E., Hayakawa, Y., Zimmermann, R., Bauer, E., Klövekorn, W.P., and Schaper, J. (2003). Myocytes die by multiple mechanisms in failing human hearts. Circ. Res. *92*, 715–724.

13. Sciarretta, S., Volpe, M., and Sadoshima, J. (2014). Mammalian target of rapamycin signaling in cardiac physiology and disease. Circ. Res. *114*, 549–564.

14. Balasubramanian, S., Johnston, R.K., Moschella, P.C., Mani, S.K., Tuxworth, W.J., Jr., and Kuppuswamy, D. (2009). mTOR in growth and protection of hypertrophying myocardium. Cardiovasc. Hematol. Agents Med. Chem. *7*, 52–63.

15. Saxton, R.A., and Sabatini, D.M. (2017). mTOR signaling in growth, metabolism, and disease. Cell *169*, 361–371.

16. Wilkins, B.J., Dai, Y.-S., Bueno, O.F., Parsons, S.A., Xu, J., Plank, D.M., Jones, F., Kimball, T.R., and Molkentin, J.D. (2004). Calcineurin/NFAT coupling participates in pathological, but not physiological, cardiac hypertrophy. Circ. Res. *94*, 110–118.

17. Egan, D.F., Chun, M.G.H., Vamos, M., Zou, H., Rong, J., Miller, C.J., Lou, H.J., Raveendra-Panickar, D., Yang, C.-C., Sheffler, D.J., et al. (2015). Small molecule inhibition of the autophagy kinase ULK1 and identification of ULK1 substrates. Mol. Cell *59*, 285–297.

18. Pyo, J.-O., Nah, J., and Jung, Y.-K. (2012). Molecules and their functions in autophagy. Exp. Mol. Med. *44*, 73–80.

19. Kim, J., Kundu, M., Viollet, B., and Guan, K.-L. (2011). AMPK and mTOR regulate autophagy through direct phosphorylation of Ulk1. Nat. Cell Biol. *13*, 132–141.

20. Dossou, A.S., and Basu, A. (2019). The emerging roles of mTORC1 in macromanaging autophagy. Cancers *11*, 1422.

21. Sciarretta, S., Forte, M., Frati, G., and Sadoshima, J. (2018). New insights into the role of mTOR signaling in the cardiovascular system. Circ. Res. *122*, 489–505.

22. Shioi, T., McMullen, J.R., Tarnavski, O., Converso, K., Sherwood, M.C., Manning, W.J., and Izumo, S. (2003). Rapamycin attenuates load-induced cardiac hypertrophy in mice. Circulation *107*, 1664–1670.

23. McMullen, J.R., Sherwood, M.C., Tarnavski, O., Zhang, L., Dorfman, A.L., Shioi, T., and Izumo, S. (2004). Inhibition of mTOR signaling with rapamycin regresses established cardiac hypertrophy induced by pressure overload. Circulation *109*, 3050–3055.

24. Morales, C.R., Li, D.L., Pedrozo, Z., May, H.I., Jiang, N., Kyrychenko, V., Cho, G.W., Kim, S.Y., Wang, Z.V., Rotter, D., et al. (2016). Inhibition of class I histone deacetylases blunts cardiac hypertrophy through TSC2-dependent mTOR repression. Sci. Signal. *9*, ra34.

25. Shende, P., Plaisance, I., Morandi, C., Pellieux, C., Berthonneche, C., Zorzato, F., Krishnan, J., Lerch, R., Hall, M.N., Rüegg, M.A., et al. (2011). Cardiac raptor ablation impairs adaptive hypertrophy, alters metabolic gene expression, and causes heart failure in mice. Circulation *123*, 1073–1082.

26. Zhang, D., Contu, R., Latronico, M.V.G., Zhang, J., Rizzi, R., Catalucci, D., Miyamoto, S., Huang, K., Ceci, M., Gu, Y., et al. (2010). MTORC1 regulates cardiac function and myocyte survival through 4E-BP1 inhibition in mice. J. Clin. Invest. *120*, 2805–2816.

27. Taneike, M., Nishida, K., Omiya, S., Zarrinpashneh, E., Misaka, T., Kitazume-Taneike, R., Austin, R., Takaoka, M., Yamaguchi, O., Gambello, M.J., et al. (2016). mTOR hyperactivation by ablation of

tuberous sclerosis complex 2 in the mouse heart induces cardiac dysfunction with the increased number of small mitochondria mediated through the down-regulation of autophagy. PLoS One *11*, e0152628.

28. Manser, E., and Lim, L. (1999). Roles of PAK family kinases. Prog. Mol. Subcell. Biol. *22*, 115–133.

29. Kumar, R., Sanawar, R., Li, X., and Li, F. (2017). Structure, biochemistry, and biology of PAK kinases. Gene *605*, 20–31.

30. Liu, W., Zi, M., Tsui, H., Chowdhury, S.K., Zeef, L., Meng, Q.-J., Travis, M., Prehar, S., Berry, A., Hanley, N.A., et al. (2013). A novel immunomodulator, FTY-720 reverses existing cardiac hypertrophy and fibrosis from pressure overload by targeting NFAT (nuclear factor of activated T-cells) signaling and periostin. Circ. Heart Fail. *6*, 833–844.

31. Liu, W., Zi, M., Naumann, R., Ulm, S., Jin, J., Taglieri, D.M., Prehar, S., Gui, J., Tsui, H., Xiao, R.-P., et al. (2011). Pak1 as a novel therapeutic target for antihypertrophic treatment in the heart. Circulation *124*, 2702–2715.

32. Tsui, H., Zi, M., Wang, S., Chowdhury, S.K., Prehar, S., Liang, Q., Cartwright, E.J., Lei, M., Liu, W., and Wang, X. (2015). Smad3 couples Pak1 with the antihypertrophic pathway through the E3 ubiquitin ligase. Hypertension *66*, 1176–1183.

33. Binder, P., Wang, S., Radu, M., Zin, M., Collins, L., Khan, S., Li, Y., Sekeres, K., Humphreys, N., Swanton, E., et al. (2019). Pak2 as a novel therapeutic target for cardioprotective endoplasmic reticulum stress response. Circ. Res. *124*, 696–711.

34. Rane, C.K., and Minden, A. (2014). P21 activated kinases: structure, regulation, and functions. Small GTPases *5*, e28003.

35. Nakai, A., Yamaguchi, O., Takeda, T., Higuchi, Y., Hikoso, S., Taniike, M., Omiya, S., Mizote, I., Matsumura, Y., Asahi, M., et al. (2007). The role of autophagy in cardiomyocytes in the basal state and in response to hemodynamic stress. Nat. Med. *13*, 619–624.

36. Tanida, I., Ueno, T., and Kominami, E. (2008). LC3 and autophagy. In Autophagosome and phagosome (Springer), pp. 77–88.

37. Thévenot, E., Moreau, A.W., Rousseau, V., Combeau, G., Domenichini, F., Jacquet, C., Goupille, O., Amar, M., Kreis, P., Fossier, P., and Barnier, J.V. (2011). p21-Activated kinase 3 (PAK3) protein regulates synaptic transmission through its interaction with the Nck2/Grb4 protein adaptor. J. Biol. Chem. *286*, 40044–40059.

38. Li, K., Wada, S., Gosis, B.S., Thorsheim, C., Loose, P., and Arany, Z. (2022). Folliculin promotes substrate-selective mTORC1 activity by activating RagC to recruit TFE3. PLoS Biol. *20*, e3001594.

39. Lim, H., Lim, Y.-M., Kim, K.H., Jeon, Y.E., Park, K., Kim, J., Hwang, H.-Y., Lee, D.J., Pagire, H., Kwon, H.J., et al. (2018). A novel autophagy enhancer as a therapeutic agent against metabolic syndrome and diabetes. Nat. Commun. *9*, 1438–1514.

40. Kim, J., Park, K., Kim, M.J., Lim, H., Kim, K.H., Kim, S.-W., Lee, E.-S., Kim, H.H., Kim, S.J., Hur, K.Y., et al. (2021). An autophagy enhancer ameliorates diabetes of human IAPP-transgenic mice through clearance of amyloidogenic oligomer. Nat. Commun. *12*, 183–215.

41. Liu, H., Liu, K., and Dong, Z. (2021). The role of p21-activated kinases in cancer and beyond: where are we heading? Front. Cell Dev. Biol. *9*, 641381.

42. Meng, J., Meng, Y., Hanna, A., Janus, C., and Jia, Z. (2005). Abnormal long-lasting synaptic plasticity and cognition in mice lacking the mental retardation gene Pak3. J. Neurosci. *25*, 6641–6650.

43. Duarte, K., Heide, S., Poëa-Guyon, S., Rousseau, V., Depienne, C., Rastetter, A., Nava, C., Attié-Bitach, T., Razavi, F., Martinovic, J., et al. (2020). PAK3 mutations responsible for severe intellectual disability and callosal agenesis inhibit cell migration. Neurobiol. Dis. *136*, 104709.

44. Holderness Parker, N., Donninger, H., Birrer, M.J., and Leaner, V.D. (2013). p21-activated kinase 3 (PAK3) is an AP-1 regulated gene contributing to actin organisation and migration of transformed fibroblasts. PLoS One *8*, e66892.

45. Shao, W., Azam, Z., Guo, J., and To, S.S.T. (2022). Oncogenic Potential of PIK3CD in Glioblastoma Is Exerted through Cytoskeletal Proteins PAK3 and PLEK2 (Laboratory Investigation), pp. 1–9.

46. Xie, J., and Xu, B. (2017). PAK3 Aggravates Pathological Cardiac Hypertrophy in Mice (OXFORD UNIV PRESS GREAT CLARENDON ST, OXFORD OX2 6DP, ENGLAND)), p. 460.

47. Mizushima, N., Yoshimori, T., and Levine, B. (2010). Methods in mammalian autophagy research. Cell *140*, 313–326.

48. Chauvin, C., Koka, V., Nouschi, A., Mieulet, V., Hoareau-Aveilla, C., Dreazen, A., Cagnard, N., Carpentier, W., Kiss, T., Meyuhas, O., and Pende, M. (2014). Ribosomal protein S6 kinase activity controls the ribosome biogenesis transcriptional program. Oncogene *33*, 474–483.

49. Yang, Q., Inoki, K., Kim, E., and Guan, K.-L. (2006). TSC1/TSC2 and Rheb have different effects on TORC1 and TORC2 activity. Proc. Natl. Acad. Sci. USA *103*, 6811–6816.

50. Simonson, B., Subramanya, V., Chan, M.C., Zhang, A., Franchino, H., Ottaviano, F., Mishra, M.K., Knight, A.C., Hunt, D., Ghiran, I., et al. (2017). DDiT4L promotes autophagy and inhibits pathological cardiac hypertrophy in response to stress. Sci. Signal. *10*, eaaf5967.

51. Ling, N.X.Y., Kaczmarek, A., Hoque, A., Davie, E., Ngoei, K.R.W., Morrison, K.R., Smiles, W.J., Forte, G.M., Wang, T., Lie, S., et al. (2020). mTORC1 directly inhibits AMPK to promote cell proliferation under nutrient stress. Nat. Metab. *2*, 41–49.

52. Blagosklonny, M.V. (2019). Rapamycin for longevity: opinion article. Aging (Albany NY) *11*, 8048–8067.

53. Li, J., Kim, S.G., and Blenis, J. (2014). Rapamycin: one drug, many effects. Cell Metabol. *19*, 373–379.

54. Arriola Apelo, S.I., Neuman, J.C., Baar, E.L., Syed, F.A., Cummings, N.E., Brar, H.K., Pumper, C.P., Kimple, M.E., and Lamming, D.W. (2016). Alternative rapamycin treatment regimens mitigate the impact of rapamycin on glucose homeostasis and the immune system. Aging Cell *15*, 28–38.

55. Settembre, C., Di Malta, C., Polito, V.A., Garcia Arencibia, M., Vetrini, F., Erdin, S., Erdin, S.U., Huynh, T., Medina, D., Colella, P., et al. (2011). TFEB links autophagy to lysosomal biogenesis. Science *332*, 1429–1433.

56. Ou, Q., Jacobson, Z., Abouleisa, R.R.E., Tang, X.-L., Hindi, S.M., Kumar, A., Ivey, K.N., Giridharan, G., El-Baz, A., Brittian, K., et al. (2019). Physiological biomimetic culture system for pig and human heart slices. Circ. Res. *125*, 628–642.

57. Jungmann, A., Leuchs, B., Rommelaere, J., Katus, H.A., and Müller, O.J. (2017). Protocol for efficient generation and characterization of adeno-associated viral vectors. Hum. Gene Ther. Methods *28*, 235–246.

58. Bolger, A.M., Lohse, M., and Usadel, B. (2014). Trimmomatic: a flexible trimmer for Illumina sequence data. Bioinformatics *30*, 2114–2120.

59. Dobin, A., Davis, C.A., Schlesinger, F., Drenkow, J., Zaleski, C., Jha, S., Batut, P., Chaisson, M., and Gingeras, T.R. (2013). STAR: ultrafast universal RNA-seq aligner. Bioinformatics *29*, 15–21.

60. Love, M.I., Huber, W., and Anders, S. (2014). Moderated estimation of fold change and dispersion for RNA-seq data with DESeq2. Genome Biol. *15*, 550–621.

61. Gillespie, M., Jassal, B., Stephan, R., Milacic, M., Rothfels, K., Senff-Ribeiro, A., Griss, J., Sevilla, C., Matthews, L., Gong, C., et al. (2022). The reactome pathway knowledgebase 2022. Nucleic Acids Res. *50*, D687–D692.

STAR★METHODS

KEY RESOURCES TABLE

REAGENT or RESOURCE	SOURCE	IDENTIFIER
Antibodies		
Flag 1:1000	Sigma	Cat# F1804; RRID:AB_262044
alphaB-Crystallin 1:100	Enzo Life Sciences	Cat# ADI-SPA-223; RRID:AB_10615646
LC3 1:100 or 1:1000	Cell Signaling	Cat# 4108; RRID:AB_2137703
PAK3 1:1000	Cell Signaling	Cat# 2609; RRID:AB_2225298
pPAK3(S154) 1:1000	Antibodies.com	Cat# A94421
BNP 1 :1000	Santa Cruz Biotechnology	Cat# sc-271185; RRID:AB_10609757
Folliculin 1;1000	Novus Biologicals	Cat# NBP1-44995SS; RRID:AB_10008585
GAPDH 1:2000	Cell Signaling	Cat# 51332; RRID:AB_2799390
SQSTM1 1:1000	Cell Signaling	Cat# 39749; RRID:AB_2799160
pULK1(S555) 1:500	Cell Signaling	Cat# 5869; RRID:AB_10707365
pULK1(S757) 1:1000	Cell Signaling	Cat# 6888; RRID:AB_10829226
ULK1 1:1000	Cell Signaling	Cat# 8054; RRID:AB_11178668
BECN1 1:1000	Cell Signaling	Cat# 3495; RRID:AB_1903911
ATG12 1:1000	Cell Signaling	Cat# 4180; RRID:AB_1903898
Tubulin 1:1000	Sigma-Aldrich	Cat# T6199; RRID:AB_477583
pMTOR(S2448) 1:1000	Cell Signaling	Cat# 2971; RRID:AB_330970
MTOR 1:1000	Cell Signaling	Cat# 2983; RRID:AB_2105622
pAMPK(T172) 1:1000	Cell Signaling	Cat# 2535; RRID:AB_331250
AMPK 1:1000	Cell Signaling	Cat# 2532; RRID:AB_330331
TEFB 1:500	Santa Cruz Biotechnology	Cat# sc-166736; RRID:AB_2255943
V5 1:1000	Cell Signaling	Cat# 13202; RRID:AB_2687461
Gβ: 1:500	Santa Cruz Biotechnology	Cat# sc-166123; RRID:AB_2109632
Troponin (T-C) 1:25	Santa Cruz Biotechnology	Cat# sc-8121; RRID:AB_2287642
α-actinin 1:500	Sigma-Aldrich	Cat# A7811; RRID:AB_476766
Anti-mouse AlexaFluor488 1:200	Jackson ImmunoResearch	Cat# 715-586-151; RRID:AB_2340858
Anti-rabbit AlexaFluor594 1:200	Jackson ImmunoResearch	Cat# 715-585-150; RRID:AB_2340854
Anti-rat AlexaFluor594 1:200	Jackson ImmunoResearch	Cat# 712-585-153; RRID:AB_2340689
HRP-linked anti-mouse 1:2000	Cell Signaling Technology	Cat# 7076, RRID:AB_330924
HRP-linked anti-rabbit 1:2000	Cell Signaling Technology	Cat# 7074; RRID:AB_2099233
HRP-linked anti-rat 1:2000	Abcam	Cat# ab102182; RRID:AB_10711694
Bacterial and virus strains		
AAV9-cTnT-Flag-Pak3	Laboratory of Olliver Muller	N/A
AAV9-cTnT-Gfp	Laboratory of Olliver Muller	N/A
Biological samples		
Human myocardial protein extracts	Asterand (US lab, Hertfordshire, UK)	N/A
Human cultured heart tissue	Laboratory of Tamer Mohamed (Ou et al., 2019) and Novabiosis (USA transplantation network)	N/A
Chemicals, peptides, and recombinant proteins		
MSL-7	Axon MedChem	2932, CAS [2172949-70-9]
Isoprenaline	Sigma	Cat# I6504

(*Continued on next page*)

Continued

REAGENT or RESOURCE	SOURCE	IDENTIFIER
Isoflurane	Isothesia, Henry Schein	N/A
Bouin's Solution	Sigma-Aldrich	Cat# HT10132
Harris' Hematoxylin	RA lamb Dry Chemical Stains	Cat# LAMB/230
Red Solution	Sigma-Aldrich	Cat# HT151
Aniline Blue	Sigma-Aldrich	Cat# B8563
Eukitt	Sigma-Aldrich	Cat# 03989
Eosin	Thermo Scientific	Cat# 6766007
VectaShield Antifade Mounting medium with DAPI	Vector laboratories	Cat# H-1000
Dialysis tube	Medicell	pore size 24 Angstrom
ProLong Glass	Thermo Fisher Scientific	Cat# P36982
DMEM, high glucose	Gibco	Cat# 41965-039
Collagenase A	Roche	Cat# 10103586001
Pancreatin	Sigma-Aldrich	Cat# P3292
Lipofectamine LTX	Invitrogen	Cat# 15300-100
Lipofectamine 2000 Reagent	Invitrogen	Cat# 11668-019
Medium 199	Gibco	Cat# 21151030
mTSER Plus	Stem Cell Technologies	Cat# 100-0276
Geltrex	Life Technologies	Cat# A1413302
CHIR99021	Millipore	Cat# 361559
IWP2	Millipore	Cat# 681671
RPMI1640	Life Technologies	Cat# 72400021
B27 minus insulin	Life Technologies	Cat# A1895601
B27 supplement	Life Technologies	Cat# 17504044
EBSS	Gibco	Cat# 24010043
Bradford Assay	BioRad	Cat# 500-0006
Pierce Protein G Agarose beads	Life Technology	Cat# 20398
Protease & phosphatase inhibitor cocktail	Merck	Cat# PPC1010
Rapamycin	Stratech	Cat# S1039-SEL
AICAR	Bio-techne	Cat# 2840
Chloroquine	Bio-techne	Cat# 4109
Bafilomycin A	Stratech	Cat# A8627-APE
Critical commercial assays		
QuikChange II kit	Agilent	Cat# 200523
Proteostat Aggresome Detection Kit	Enzo Life Science	Cat# ENZ-51035-K100
PicoProbe™ LDH-Cytotoxicity Fluorometric Assay Kit	BioVision	Cat# K314-500
Lactate Dehydrogenase Activity Assay Kit	Sigma	Cat# MAK066
in situ Cell death detection kit	Roche	Cat# 11684795910
DNA-free Removal Kit	Invitrogen	Cat# AM1906
LunaScript RT-PCR	New England Biolabs	Cat# NEB3010
SYBR Select PCR master mix	Applied Biosystems	Cat# 4472908
ECL Prime	Amersham	Cat# RPN2232
ECL Select	Amersham	Cat# RPN2235

(*Continued on next page*)

Continued

REAGENT or RESOURCE	SOURCE	IDENTIFIER
Experimental models: Cell lines		
HEK293A	Invitrogen	Cat# R70507
H9C2 cells	European Collection of Authenticated Cell cultures	Cat# 88092904; RRID:CVCL_0286
Experimental models: Organisms/strains		
Mouse: C57BL/6J	Envigo, UK	RRID:IMSR_JAX:000664/
Rat: Sprague-Dawley Rats	Envigo,UK	RRID:RGD_737903
Oligonucleotides		
F Not1-Pak3 to 3xflag primer	Sigma-Aldrich	tcagtcgcggccgcgatgtctgacggtctggat
R BamH1-Pak3 stop to Flag primer	Sigma-Aldrich	tcagtcggatccttagcggctgctgttcttaat
F Age1-Kozac-Flag-Pak3 to pSSV9 primer	Sigma-Aldrich	tcagtcaccggtgccaccatggactacaaagaccatgac
R FseI-Pak3 stop to pSSV9 primer	Sigma-Aldrich	tcagtcggccggccttagcggctgctgttcttaat
F Kpn1-Pak3 to pEntr11 primer	Sigma-Aldrich	tcagtcggtaccatgtctgacggtctggat
R Not1-NOstop Pak3 to pENTR11 primer	Sigma-Aldrich	tcagtcgcggccgcacgcggctgctgttcttaat
Pak3 Threonine 421 to Glutamate primer	Sigma-Aldrich	gcaaagtaaacgaagcgagatggtgggaacccc ggggttcccaccatctcgcttcgtttactttgc
Pak3 Threonine 421 to alanine primer	Sigma-Aldrich	gcaaagtaaacgaagcgcaatggtgggaacccc ggggttcccaccattgcgcttcgtttactttgc
Scramble siRNA	Sigma-Aldrich	agguaguguaaucgccuug
Rat Pak3 siRNA	Ambion	Cat# s131407, Silencer Select Pre-Designed
Nppb qPCR primers	Qiagen	Cat# QT00107541 Quantitech primer assay
Col3a1 qPCR primers	Qiagen	Cat# QT02331301 Quantitech primer assay
Col1a2 qPCR primers	Qiagen	Cat# QT02325736 Quantitech primer assay
18S qPCR primer	Qiagen	Cat# QT02448075 Quantitech primer assay
Recombinant DNA		
R777-E151 Hs.PAK3	Addgene	RRID:Addgene_70435
pSSV9-TnT-Gfp	Laboratory of Oliver Muller (Werfel et al., 2014)	N/A
p3xFlag-CMV7.1	Sigma	N/A
pEntr11	Invitrogen	Cat# A10467
pAd/CMV/V5-DEST	Invitrogen	Cat# V493-20
ptfLC3	Addgene	RRID:Addgene_21074
Software and algorithms		
FlowJo	FlowJo LLC	https://www.flowjo.com/
GraphPad Prism 9	GraphPad Software	https://www.graphpad.com/scientific-software/prism/
ImageJ-Fiji	National Institutes of Health, USA	https://fiji.sc/
Mascot	Matrix Science	https://www.matrixscience.com/search_form_select.html
Scaffold	Proteome Software	https://www.proteomesoftware.com
LabChart 7	ADInstruments	https://www.adinstruments.com/support/software/archive
Reactome	Global Core Biodata/Elixir Infrastructure	https://reactome.org

(*Continued on next page*)

Continued

REAGENT or RESOURCE	SOURCE	IDENTIFIER
Other		
Alzet minipump	Charles River	Cat# 1002
Deposited data		
RNA-seq	This paper	Array Express: E-MTAB-12979
Proteomic	This paper	ProteomeXchange – PRIDE: PXD041986

RESOURCE AVAILABILITY

Lead contact

Further information and requests for resources and reagents should be directed to and will be fulfilled by the lead contact, Wei Liu (wei.liu@manchester.ac.uk).

Materials availability

Plasmids generated in this study are available upon request directed to the lead contact.

Data and code availability

- RNA-seq raw data have been deposited in Array Express and are publicly available as of the date of publication. Mass spectrometry data have been deposited to the ProteomeXchange Consortium and are publicly available as of the date of publication. The accession numbers are listed in the key resources table.
- This paper does not report any original code.
- Any additional information required to reanalyze the data reported in this paper is available from the lead contact upon request.

EXPERIMENTAL MODEL AND SUBJECT DETAILS

Human heart protein extracts

Human myocardial protein extracts from both male and female heart failure patients suffering from post-ischemic and dilated cardiomyopathy and normal subjects were purchased from Asterand (now part of BioIVT, UK). Asterand obtained ethical approval and consent following the United Kingdom Human Tissue Authority regulations.

Animal models

All animal studies followed the United Kingdom Animals (Scientific Procedures) Act 1986. They were approved by the University of Manchester's ethics committee and performed under the Home Office license P3A97F3D1. Mice and rats were housed in a pathogen-free facility at the University of Manchester. Ten-week-old male C57BL/6 mice and pregnant Sprague-Dawley rats were purchased from Envigo, UK. Cardiac stress was induced by isoprenaline administration (8 mg/kg/day) (I5627, Sigma-Aldrich). For the two-day study, the dose was divided into two daily injections. For the two-week study, a subcutaneous Alzet minipump (1002, Charles River) was implanted in the lower dorsal area for continuous delivery. Mice were anesthetized by 2.5% isofluorane inhalation. Analgesia was provided by subcutaneous injection of 0.1 mg/kg buprenorphine and local administration of bupivacaine (4 mg/kg) to the incision site.

Cell lines

H9C2 cells were obtained from the European Collection of Authenticated Cell cultures (Sigma-Aldrich, 88092904), while the HEK293A cells were acquired from Invitrogen (Cat# R70507). Cells were kept at 37°C with 5% CO_2 in DMEM medium (11966025, Gibco) with 10% fetal bovine serum (10500064, Gibco).

Neonatal rat ventricular myocytes isolation (NRVM)

NRVMs were isolated from 2-day-old male and female Sprague-Dawley rats. The hearts were cut into small pieces and subjected to 8–10 sequential 6 min enzyme digestion in 7ml of ADS buffer (30U/100ml Collagenase A, 116 mM NaCl, 20mM HEPES, 1 mM NaH_2PO_4, 6 mM glucose, 5 mM KCl, 0.8 mM MgSO4, pH 7.4)

supplemented by 25U/75ml Collagenase A (10103586001, Roche) and 100 mg/ml pancreatin (P3292, Sigma-Aldrich). Cardiomyocytes were separated from non-myocytes by plating them on four Petri dishes and incubating them for 1 hr at 37°C. Cardiomyocytes, cells not attached to the bottom, were collected and seeded with plating media (67% DMEM, 17% medium199, 10% horse serum, 5% fetal bovine serum, 1% penicillin-streptomycin, 1% fungizone, 1 μM bromodeoxyuridine) at the desired density. After 24hrs, plating media were aspirated and replaced by maintenance media (80% DMEM, 20% M199, 10% fetal bovine serum, 1% penicillin-streptomycin, 1% fungizone, and 1 μM bromodeoxyuridine).

Human induced pluripotent stem cells-derived cardiomyocytes (iPSC-CMs)

The iPSC cell line SEUR7 was established from human dermal fibroblasts using a CytoTune iPS Programming kit (Life Technologies) by Wellcome Trust Sanger Institute and made available via Public Health England through European Collection of Cell Cultures (ECACC) under a material transfer agreement. The cells were maintained in feeder-free culture conditions with mTSER Plus (100-0276, Stem Cell Technologies) on Geltrex-coated plates (A1413302, Life Technologies). Cardiomyocyte differentiation was achieved with 4μM CHIR99021 (361559, Millipore) incubation for 48 hr and 5μM IWP2 (681671, Millipore) for a further 48 hours in RPMI1640 HEPES Glutamax medium (72400021, Life Technologies) with B27 minus insulin supplement (A1895601, Life Technologies). Cardiomyocytes were enriched using a lactate selection medium (RPMI 1640 minus glucose, 4mM lactate, B27 supplement) for six days. iPSC-CMs were cultured in RPMI1640 HEPES Glutamax medium with B27 supplement (17504044, Life Technologies) for at least 21 days before treating. Autophagy was induced by 4-hour starvation with EBSS.

Human heart slice treatment

The Carolina Donor services provided a fresh human heart from a consented and deidentified donor. The IRB committee approved the protocol at the University of Louisville as a non-human subject research. The harvest and slicing of the heart have been described before,[56] and the treated heart protein extracts were a kind gift from Dr. Tamer M.A. Mohamed (University of Louisville). The donor was aged 37 years old with no CVD history. Briefly, the freshly sliced heart was maintained in the culture medium overnight, followed by 10 μM isoprenaline and 50 μM chloroquine for 1 hr. After collection, the protein was extracted with RIPA buffer for immunoblotting.

METHOD DETAILS

AAV9 production

The human Pak3 cDNA sequence (70435, Addgene) was cloned into the pSSV9-TnT-Gfp plasmid, removing the *Gfp* coding sequence. First, NotI and BamHI restriction sites were added to the Pak3 sequence and the PCR product was introduced to the p3xFlag plasmid (Sigma) to fuse the 3xFlag tag to the N-terminal of Pak3. After that, AgeI-Kozac and FseI sequences were incorporated by PCR to Flag-Pak3 the product was ligated to the digested pSSV9-TnT-Gfp plasmid. The primer sequences can be found in the key resources table. Viral packaging was performed by Oliver Muller, and the detailed process has been described before.[57] Briefly, the gene of interest plasmid was co-transfected into low passage HEK293T cells along with the adenoviral helper plasmid (pDGDVP) and the pAAV2-9 Rep-Cap plasmid (p5E18-VD2/9). Recombinant AAV9 was purified by discontinuous iodixanol gradient ultracentrifugation and titrated by qPCR. PAK3 overexpression was induced by tail vein injection of the viral vector AAV9-cTnT-Flag-*Pak3* ($1x10^{11}$ viral particles), and AAV9-cTnT-*Gfp* was injected as vehicle control.

MSL-7 administration

The autophagy inducer MSL-7 (2932, CAS [2172949-70-9]) was purchased from Axon Medchem. To test its working concentration, we referred to the previous study,[39] trying its effects on H9C2 cells by using gradually increased doses, such as 1, 10, 50, and 100μM. For the *in vitro* experiment in main figures, a stock of 10mM was prepared in DMSO, and directly added the culture medium for a final concentration of 10 μM 4 hours before collection. For *in vivo* administration, it was dissolved in DMSO to a concentration of 125 mg/ml. We tested its effects on cardiac function using two doses, 50 mg/kg and 100 mg/kg, both of which worked to improve cardiac performance in PAK3-overexpressed hearts. Thus, for the subsequent experiments, the stock was diluted to 62.5 mg/ml with more DMSO on the injection day. Doses of 50 mg/kg were administered via IP thrice a week for two weeks. Similar DMSO volumes were used as vehicle controls.

Echocardiography

For cardiac function evaluation, mice were anesthetized with 1.5% isofluorane (Isothesia, Henry Schein), and ultrasound imaging was performed with an Acuson Sequoia C256 system (Siemens). Ventricular dimensions were measured from M-mode images, while IVRT and E/A were measured from pulse wave Doppler images.

RNA-sequencing

Total RNA was extracted from whole hearts of C57BL/6 mice 12 weeks after TAC or Sham, with two individuals per group. The quality and integrity of total RNA samples were checked using a 2100 Bioanalyzer (Agilent Technologies). RNA-seq libraries were then generated using the TruSeq Stranded mRNA assay (Illumina) according to the manufacturer's instructions. Unmapped paired reads of 76 bp were interrogated using a quality control pipeline comprising FastQC v0.11.3 and FastQ Screen v0.9.2. The reads were trimmed to remove any adapter or poor-quality sequence using Trimmomatic v0.36.[58] Furthermore, the reads were truncated at a sliding four-bp window with a mean quality <Q20. Afterward, filtered reads were mapped to the mouse reference sequence analysis set (mm10/Dec. 2011/GRCm38) from the UCSC browser using STAR v2.5.3a.[59] The genome index was created using the MouseGencode M16 gene annotation. Correctly mapped reads were counted using htseq-count v0.6.1p1. Normalization and differential expression analysis were performed using DESeq2v1.10.1 on Rv3.2.3 (http://www.R-project.org/).[60] The genes with significantly different expressions were determined by false discovery rate errors of less than 0.05 for the absolute value of a $\log_2$ fold change.

Mass spectrometry

Mass spectrometry was used to investigate PAK3 protein interactors by identifying proteins immunoprecipitated with PAK3. 3xFlag-PAK3 was overexpressed in HEK293 cells by plasmid transfection. After 72 hrs, cells were quickly fixed with 0.4% paraformaldehyde (PFA) prepared in PBS. The protein was extracted with RIPA buffer (50 mM Tris-HCl, 150 mM NaCl, 0.1% SDS, 0.5% sodium deoxycholate, 1 mM EDTA, 1% NP-40, 25 mM glycerophosphate, protease & phosphatase inhibitor cocktail (PPC1010, Merck)). PAK3 and its interactors were immunoprecipitated using an Anti-Flag antibody (F1804, Sigma) crosslinked to Pierce Protein G Agarose (20398, Life Technologies) following the manufacturer's instructions. Approximately 1 mg of input protein was used. Immune complexes were eluted using 2xLaemmli sample buffer (125 mM Tris-HCl, 4% SDS, 20% glycerol, 0.01% bromophenol blue, 10% β-mercaptoethanol, pH6.8). Precipitated proteins were run for 5 min in SDS-PAGE, and the whole bands were excised. After acetonitrile dehydration, the gel pieces were reduced and alkylated with 10 mM dithiothreitol and 55 mM iodoacetamide, respectively. In-gel digestion was performed overnight at 37°C with trypsin. The resulting peptides were analyzed by LC-MS/MS using an UltiMate® 3000 Rapid Separation LC (RSLC, Dionex Corporation, Sunnyvale, CA) coupled to an Orbitrap Elite (Thermo Fisher Scientific, Waltham, MA) mass spectrometer. Peptide mixtures were separated using a gradient from 92% A (0.1% FA in water) and 8% B (0.1% FA in acetonitrile) to 33% B in 44 min at 300 nL min-1, using a 75 mm × 250 μm i.d. 1.7 mM BEH C18, analytical column (Waters). Peptides were selected for fragmentation automatically by data dependant analysis. Protein identification was performed using the Mascot (Matrix Science) software, searching against a human Swissprot proteome database. Data were validated using Scaffold (Proteome Software, Portland, OR), and protein abundances were used for pathway analysis with the Reactome database.[61]

Blood pressure

Blood pressure was measured on conscious mice by a non-invasive tail-cuff system (CODA, Kent Scientific Corporation). Measurements were performed at the same time of day, and ten acclimation cycles were discarded before starting to record. At least eight measurements were averaged per mouse. Systolic blood pressure, diastolic blood pressure, tail blood volume, tail blood flow, and heart rate were recorded for each mouse.

Histology

Immediately after dissection, the hearts were fixed in 4% PFA for 4 hr at 4°C. They were subsequently washed with PBS for 30 mins and dehydrated in 50%, 70%, 90%, and 100% ethanol for 2 hr each. The hearts were finally cleared in xylene overnight, followed by paraffin infiltration. Blocks were trimmed and sectioned into 5 mm sections.

Masson's trichrome

Fibrotic tissue was differentiated by Masson's Trichrome staining. Heart sections were dewaxed, rehydrated, and fixed for 2 hr in Bouin's Solution (HT10132, Sigma), followed by nuclear staining with Harry's Hematoxylin (LAMB/230, RA Lamb Dry Chemical Stains) for five mins. Subsequently, Red Solution (HT151, Sigma) and Aniline Blue (B8563, Sigma) incubations were performed to stain muscle and collagen fibers, respectively. Finally, sections were dehydrated in ethanol and xylene baths and mounted with the xylene-based medium, Eukitt (03989, Sigma). Brightfield images were captured with a D-Histech Panoramic-250 microscope slidescanner, and the fibrotic area was measured using ImageJ.

Hematoxylin and eosin

Cardiomyocyte cross-sectional area was calculated from H and E-stained myocardial paraffin sections. After dewaxing and rehydration, sections were incubated in Harry's Haematoxylin (LAMB/230, RA Lamb Dry Chemical Stains) for five mins, followed by differentiation with 1% HCl prepared in 70% (v/v) ethanol for 10 secs. Blueing was achieved by washing with warm running tap water, followed by Eosin (6766007, Thermo Fisher Scientific) counterstain for 1 min. Samples were dehydrated and mounted with Eukitt. Brightfield images were captured with a D-Histech Panoramic-250 microscope slidescanner. Ten fields were acquired per sample for quantification, and images were analyzed using ImageJ. Approximately 5,000 cardiomyocytes were measured per heart.

TUNEL

Apoptosis was detected in heart sections by staining with DAPI and TUNEL (*In Situ* Cell Death Detection Kit, Roche). TUNEL was performed following the manufacturer's instructions and finally mounted with DAPI-containing Vectashield (H-1200, Vector Laboratories). Fluorescent images were acquired with an Axio Imager.M2 [Zeiss]upright microscope, and a Coolsnap EZ camera (Photometrics). Specific band pass filter sets for DAPI and FITC were used. Ten fields were acquired per sample for quantification, and images were analyzed using ImageJ. At least 2,000 nuclei were counted per heart.

Immunohistochemistry

Paraffin heart sections were dewaxed with xylene and rehydrated in decreasing ethanol concentrations for 5 min each. Slides were heated to 95°C in sodium citrate buffer (10 mM Sodium citrate, 0.05% Tween 20, pH 6.0) for 20 min. The sections were blocked with 10% normal goat serum in 0.1% Triton-X in PBS and then incubated with anti-alphaB-Crystallin antibody (ADI-SPA-223, Enzo Life Sciences) diluted 1:100 and incubated overnight at 4°C. The samples were washed with PBS, and a mixture of 0.3% H_2O_2 in PBS was used to block endogenous peroxidase activity for 15 min. Next, slides were incubated with HRP-linked goat anti-rabbit diluted 1:1,000 (7074, Cell Signaling) for 2 h at room temperature. After washing, the signal was developed using diaminobenzidine (DAB) as peroxidase substrate, and nuclei were counterstained Harris' Hematoxylin for 7 min. Finally, the slides were dehydrated and mounted with Eukitt. Brightfield images were captured with a D-Histech Panoramic-250 microscope slidescanner, and the quantification was performed with the IHC profiler plug-in for ImageJ. The reported positive cells include the low, medium, and high positive cells.

Adenovirus production and cell transduction

The human *Pak3* cDNA sequence was subcloned into the pEntr11 plasmid (A10467, Invitrogen). Site-directed mutagenesis was used to mutate T421 to glutamate (E) or alanine (A) to obtain a constitutively active or a dead kinase, respectively. The employed primers were 5′- gcaaagtaaacgaagcgagatggtgggaacccc-3′ and 5′-ggggttcccaccatctcgcttcgtttactttgc-3′ for the former, and 5′-gcaaagtaaacgaagcgcaatggtgggaacccc-3′ and 5′-ggggttcccaccattgcgcttcgtttactttgc-3′ for the latter. The QuikChange II kit (200523, Agilent) was used for the procedure following the supplier's recommended protocol. The sequence was recombined to pAd/CMV/V5-DEST (V493-20, Invitrogen), fusing *Pak3* to V5 tag, and the resulting plasmid was introduced to HEK293A cells (R70507, Invitrogen) to produce the adenovirus vector. After harvesting, the viral vector was purified by discontinuous cesium chloride gradient (1.33 g/ml and 1.45 g/ml) and dialysis (pore size 24 Angstrom, Medicell). For PAK3 overexpression *in vitro*, cells were transduced using a multiplicity of infection (MOI) of 25 for 48 hr before further treatment.

mCherry-Gfp-LC3 expressing H9C2 cell line

The dual reporter mCherry-Gfp-LC3 in the ptfLC3 plasmid was used to detect the fusion of autophagosomes to lysosomes for degradation. H9C2 cells were authenticated by the ATCC and tested negative for mycoplasma regularly. The ptfLC3 plasmid (21074, Addgene) was transfected with Lipofectamine 2000 Reagent (11668–019, Invitrogen). Cells were incubated for 48 hr at 37°C with 5% CO_2 before starting neomycin selection for one week. Cells were dissociated and seeded on a 96-well plate individually. Four clones were selected under the microscope for fluorescent LC3 expression and evaluated for autophagy response with starvation. Cells were continued to be cultured with neomycin to maintain the reporter expression until the start of flow cytometry experiments. For microscopy visualization after treatment, cells were fixed with 4% PFA for 10 min at room temperature and mounted with ProLong Glass (P36982, Thermo Fisher Scientific). Fluorescent images were acquired with an Axio Imager M2 (Zeiss) upright microscope and a Coolsnap EZ camera (Photometrics). Specific band pass filter sets for FITC and Texas Red were used.

siRNA transfection

Pak3 knockdown *in vitro* was achieved with Lipofectamine LTX & Plus Reagent (15338-100, Invitrogen) transfection of Silencer Select Pre-Designed rat si*Pak3* siRNA (s131407, Ambion). The cells were incubated with 100 nM of the siRNA complexes for 48 hr at 37°C with 5% CO_2 before further treatment.

Flow cytometry

To quantify the effects of PAK3 overexpression on autophagic flux, the mCherry-Gfp-LC3 cells reporter was measured by flow cytometry. After treatment, the cells were trypsinized by incubating with TrypLE Express (12605036, Thermo Fisher Scientific) for 1–2 min at 37°C. Immediately cold DMEM (11966025, Gibco) with 10% fetal bovine serum (10500064, Gibco) was added, and the cells were transferred to Eppendorf tubes. After centrifuging for 5 min at 100xg, the medium was removed, and cells were resuspended with 500 μl of PBS. The samples were kept cold from harvesting until analysis and passed through a 70 μm Flowmi strainer (BAH136800070, Bel-Art). They were run on a FACSymphony (BD Biosciences) with BDFACS software. Data was collected from the 488 530/30 and 561 610/20 channels. The data was analyzed using the FlowJo v10 software. Singles cells were gated from forward, and side scatter dot blots. Afterward, fluorescent cells were gated using a non-transfected negative control and dynamic cells by testing with the autophagy inducer rapamycin and the inhibitor chloroquine. The derived parameter mCherry-Gfp was calculated as the ratio of the red signal over the green signal. From this parameter, cells were divided into two populations, low and high autophagy cells, based on the initial testing with the inducer and inhibitor. The percentage of high autophagy cells was used to compare the samples.

Cells treatments

Different inducers and inhibitors were employed to evaluate the autophagy response *in vitro*. The molecules were added to fresh DMEM medium (11966025, Gibco) with 10% fetal bovine serum (10500064, Gibco) and incubated for 2 hr at 37°C with 5% CO_2 before collection. The treatments included 5 μM rapamycin (S1039-SEL, Stratech), 1 mM AICAR (2840, Bio-techne), 50 μM Chloroquine (4109, Bio-techne), 50 nM Bafilomycin A (A8627-APE, Stratech), and 10 μM isoprenaline (I5627, Sigma-Aldrich).

Immunofluorescent staining

LC3 detection and TUNEL with troponin staining were performed on iPSC-CMs. After EBSS starvation for 4 hours, they were fixed with 4% PFA for 15 min at room temperature, followed by permeabilization with 0.1% Triton X + 0.1% sodium citrate for 8 min on ice. TUNEL was performed before immunodetection on corresponding samples. Coverslips were then incubated for 1 hr in 10% normal donkey serum. Anti-LC3 (4108, Cell Signaling) and anti-cTnT (8121, Santa Cruz Biotechnology) antibodies were diluted 1:100 and 1:25, respectively, and applied to coverslips for incubation overnight at 4°C. The secondary donkey anti-rabbit-Alexa-594 antibody (715-585-150, Jackson ImmunoResearch) was used after washing with PBS. Finally, the coverslips were incubated with DAPI-PBS solution for 5 min and washed again with PBS. Coverslips were mounted with ProLong Glass (P36982, Thermo Fisher Scientific). Fluorescent images were acquired with an Axio Imager M2 (Zeiss) upright microscope and a Coolsnap EZ camera (Photometrics) with a specific bandpass filter set for DAPI, FITC, and Texas Red.

Protein aggregate detection

Protein aggregates in iPSC-CMs were detected with the Proteostat Aggresome Detection Kit (Enzo Life Science, ENZ-51035-K100). Cells were fixed with 4% PFA for 15 min at room temperature and permeabilized with 0.1% Triton X + 0.1% sodium citrate for 8 min on ice. The dual detection reagent was prepared by diluting the Proteostat detection reagent and Hoechst 33342 nuclear stain 1:1,000 in the buffer provided. Cells were incubated with the detection reagent for 30 min at room temperature before washing with PBS and mounting with ProLong Glass (P36982, Thermo Fisher Scientific). Fluorescent images were acquired with an Axio Imager M2 (Zeiss) upright microscope and a Coolsnap EZ camera (Photometrics) with a specific bandpass filter set for DAPI, FITC, and Texas Red.

LDH assay

LDH level in cell culture medium was measured using PicoProbe™ LDH-Cytotoxicity Fluorometric Assay Kit (K314-500, BioVision). LDH activity in serum was measured by colorimetric assay (MAK066, Sigma). Serum was prepared by allowing blood to clot for 1 hr at room temperature and centrifuging for 15 mins at 6,000xg. The assays were performed following the manufacturer's instructions.

Immunoblotting analysis

For Western Blots, total protein lysates from ventricular tissue or cells were prepared with Triton lysis buffer (137 mmol/L NaCl, 20 mmol/L Tris, 0.1% w/v SDS, 2 mmol/L EDTA, 10% v/v glycerol, 1% Triton X-100, 25 mmol/L glycerophosphate, protease &phosphatase inhibitor cocktail (PPC1010, Merck), pH7.4). Lysates were cleared by centrifuging, and protein concentration was quantified by Bradford assay (500-0006, Bio-Rad). A total of 30 μg of protein was subjected to SDS-PAGE in polyacrylamide gels. Immunoblot analysis was performed with the following primary antibodies: anti-PAK3 (2609, Cell Signaling),anti-pPAK3(S154) (A94421, Antibodies.com), anti-BNP (sc-271185, Santa Cruz Biotechnology), anti-GAPDH (51332, Cell Signaling), anti-Gβ (sc-166123, Santa Cruz Biotechnology), anti-SQSTM1 (39749, Cell Signaling), anti-pULK1(S555) (5869, Cell Signaling), anti-pULK1(S757) (6888, Cell Signaling), anti-ULK1 (8054, Cell Signaling), anti-BECN1 (3495, Cell Signaling), anti-ATG12 (4180, Cell Signaling), anti-LC3 (4108, Cell Signaling), anti-Tubulin (T6199, Sigma-Aldrich), anti-pMTOR (2971, Cell Signaling), anti-MTOR (2983, Cell Signaling), anti-pAMPK(T172) (2535, Cell Signaling), anti-AMPK (2532, Cell Signaling), anti-Folliculin (NBP1-44995SS,Novus Biologicals), anti-TEFB (sc-166736, Santa Cruz Biotechnology), anti-Flag (F1804, Sigma-Aldrich), anti-V5 (13202, Cell Signaling). Secondary anti-mouse (7076, Cell Signaling) and anti-rabbit (7074, Cell Signaling) HRP conjugates were used along with the Amersham ECL Prime and Select detection reagents (RPN2232 and RPN2235, Amersham) to detect the bands of interest. Images were obtained with a ChemiDoc MP System (BioRad).

Co-immunoprecipitation

To assess PAK3 interaction of Folliculin, co-immunoprecipitation was performed on Ad-*Pak3*-CA infected H9C2 cells. 48 hrs post injection, cells were fixed with 0.4% PFA, and the protein was extracted using RIPA buffer. Approximately 2 mg of input protein was used to pull out overexpressed PAK3 using Anti-V5 antibody or IgG cross-linked to Pierce Protein G Agarose. Immune complexes were eluted with 2xLaemmli sample buffer. Precipitated proteins were run in SDS-PAGE, and Immunoblot analysis was performed using anti-Folliculin antibody.

Quantitative real-time polymerase reaction (qPCR)

Total RNA from cells and ventricular tissue was obtained by Trizol extraction. Samples were treated with DNAse (AM1906, Invitrogen) to eliminate genomic DNA contamination. RNA was converted to cDNA using LunaScript RT Super Mix Kit (NEB3010, New England Biolabs). Specific primers for quantitative real-time polymerase reaction (qPCR) were purchased from Qiagen, and reactions were conducted using SYBR Select PCR Master Mix (4472908, Applied Biosystems) following the manufacturer's instructions. qPCR reactions were detected with the Step One Plus PCR System (Applied Biosystems), and the fold change was calculated by the $2^{-\Delta\Delta}$Ct method. The level of mRNA expression was normalized to 18S expression.

QUANTIFICATION AND STATISTICAL ANALYSIS

Data are presented as mean ± SEM and were analyzed using ordinary one-way or two-way ANOVA followed by post hoc tests where appropriate. Comparisons between two groups were performed using Student's t-test. Statistical analysis was performed using the GraphPad Prism 9 software. P-values <0.05 was considered statistically significant. The sample size (N) corresponds to biological replicates and is specified for each experiment in the figure legend.